



**HAL**  
open science

## The doublecortin-related gene *zyg-8* is a microtubule organizer in *Caenorhabditis elegans* neurons.

Jean-Michel Bellanger, Juan G Cueva, Renee Baran, Garland Tang, Miriam B Goodman, Anne Debant

► **To cite this version:**

Jean-Michel Bellanger, Juan G Cueva, Renee Baran, Garland Tang, Miriam B Goodman, et al.. The doublecortin-related gene *zyg-8* is a microtubule organizer in *Caenorhabditis elegans* neurons.. *Journal of Cell Science*, 2012, epub ahead of print. 10.1242/jcs.108381 . hal-00730409

**HAL Id: hal-00730409**

**<https://hal.science/hal-00730409>**

Submitted on 10 Sep 2012

**HAL** is a multi-disciplinary open access archive for the deposit and dissemination of scientific research documents, whether they are published or not. The documents may come from teaching and research institutions in France or abroad, or from public or private research centers.

L'archive ouverte pluridisciplinaire **HAL**, est destinée au dépôt et à la diffusion de documents scientifiques de niveau recherche, publiés ou non, émanant des établissements d'enseignement et de recherche français ou étrangers, des laboratoires publics ou privés.

**The Doublecortin-related Gene *zyg-8* is a Microtubule Organizer in *Caenorhabditis elegans* Neurons**

Jean-Michel Bellanger <sup>1\*</sup>, Juan G. Cueva <sup>2</sup>, Renee Baran <sup>3</sup>, Garland Tang <sup>3</sup>, Miriam B. Goodman <sup>2</sup> and Anne Debant <sup>1</sup>.

Running Title : *zyg-8* organizes neuronal microtubules

1- CRBM-CNRS

Université Montpellier 2

1919, route de Mende

34293 Montpellier

FRANCE

Ph : +33-434359516

Fax : +33-434359410

2- Department of Molecular and Cellular Physiology,

Stanford University School of Medicine,

279 Campus Dr.

Stanford, CA 94305

USA

Ph : 1-650-721-5976

Fax : 1-650-721-8021

3- Biology Department

Occidental College

1600 Campus Road,

Los Angeles, CA 90041

USA

Ph : 1-323-259-1422

Fax : 1-323-341-4974

\* Corresponding author : [jean-michel.bellanger@crbm.cnrs.fr](mailto:jean-michel.bellanger@crbm.cnrs.fr)

## Summary

Doublecortin-domain containing (*DCDC*) genes play key roles in the normal and pathological development of the human brain cortex. The origin of the cellular specialization and the functional redundancy of these microtubule (MT)-associated proteins (MAPs), especially those of Doublecortin (*DCX*) and Doublecortin-like kinase (*DCLKs*) genes, is still unclear. The *DCX* domain displays the ability to control MT architecture and bundling. However, the physiological significance of such properties is not fully understood. To address these issues, we sought post-mitotic roles of *zyg-8*, the sole representative of the *DCX-DCLK* subfamily of genes in *C. elegans*. Previously, *zyg-8* has been shown to control anaphase-spindle positioning in one-cell stage embryos, but functions of the gene later in development have not been investigated.

Here we show that wild-type *zyg-8* is required beyond early embryonic divisions for proper development, spontaneous locomotion and touch sensitivity of adult worms. Consistently, we find *zyg-8* expression in the six touch receptor neurons (TRNs), as well as in a subset of other neuronal and non neuronal cells. In TRNs and motoneurons, *zyg-8* controls cell body shape/polarity and process outgrowth and morphology. Ultrastructural analysis of mutant animals reveals that *zyg-8* promotes structural integrity, length and number of individual MTs, as well as their bundled organization in TRNs, with no impact on MT architecture.

## Introduction

The Doublecortin (DCX) family of Microtubule-Associated Proteins (MAPs) includes the X-linked lissencephaly and doublecortex syndrome *DCX* gene, the Doublecortin-like kinase *DCLK* genes, the retinitis pigmentosa *RPI* gene as well as the dyslexia-associated *DCDC2* gene (for review, see Reiner et al., 2006). This family of genes is conserved in animals, including mammals, fish, insects and nematodes. The mouse genome harbors 11 such genes, complicating functional analysis of these proteins *in vivo*. Nevertheless, considerable effort has been focused on understanding the physiopathology of DCX domain-containing proteins (DCDCs) in the mammalian nervous system, especially that of the Doublecortin and DCLKs subgroup. Thus, in mice, *DCX* and *DCLK-1* function redundantly in several types of cortical neurons to ensure their migration as well as the control of axon growth and wiring during embryonic life (Deuel et al., 2006; Koizumi et al., 2006). In addition, *DCX* and *DCLK-1* displays earlier functions in neurogenesis (Pramparo et al., 2010; Shu et al., 2006) and *DCLK-2* expression persists in mature neurons, in which it may play roles at the growth cone (Edelman et al., 2005).

Doublecortin promotes selective assembly and stability of 13-protofilament (13-pf) MTs *in vitro*, through the maintenance of lateral and longitudinal contacts between adjacent protofilaments (Fourniol et al., 2010; Moores et al., 2004). Many DCDCs also induce microtubule bundling when overexpressed in mammalian cells, suggesting that this family of proteins may also mediate intermolecular interactions between adjacent MTs (Bielas et al., 2007; Coquelle et al., 2006). To date, however, the contribution of DCDC proteins to MT organization in post-mitotic cells such as neurons is poorly documented.

We address these issues by analyzing *zyg-8* in the nematode *C. elegans*. The rationale for this choice is two-fold. First, *C. elegans* has a simple and well-characterized neuroanatomy and powerful genetic tools allow for straightforward analyses of gene function at a whole organism scale. Second, *zyg-8* is the unique representative of the *DCX-DCLK* subfamily in *C. elegans*, allowing for the analysis of evolutionary conserved functions of this group of genes. Previous studies established the essential role of *zyg-8* in mitotic spindle positioning of one-cell stage *C. elegans* embryos, a function highly reminiscent of that of *DCLK-1* in dividing murine neuronal precursor cells (Gonczy et al., 2001; Shu et al., 2006). Part of the *DCLK* properties may thus have been retained throughout metazoan evolution, although post-embryonic functions of *zyg-8* have not been investigated to date, due to early lethality of homozygous mutant embryos.

Here we show that *zyg-8* is required throughout gastrulation for proper development and survival of embryos, and later on for spontaneous locomotion and touch sensitivity of adult animals. We find that *zyg-8* is expressed in several classes of neurons, including motoneurons and touch receptor neurons (TRNs), as well as in some non-neuronal tissues. We show that *zyg-8* is required to maintain neuronal cell shape/polarity and process outgrowth/wiring in developing worms. In addition, we demonstrate that *zyg-8* promotes bundling, length and structural integrity of the atypical 15-pf MTs that fill TRN processes, without affecting MT architecture. Therefore, in *C. elegans* neurons, *zyg-8* recapitulates most functions attributed to *DCX-DCLK* genes in the mammalian brain, strongly suggesting an ancient origin for these properties.

## Results

### ***zyg-8* is required beyond the first division for full embryonic survival**

*zyg-8* null mutant animals display a penetrant, maternal-effect embryonic lethality, likely resulting from the dramatic anaphase spindle positioning defects in one-cell stage *C. elegans* embryos (Gonczy et al., 2001; Wood et al., 1980). But, it is not known what functions *zyg-8* has in development and physiology beyond the first mitotic division. To address this question, we took advantage of two conditional, temperature-sensitive alleles, *zyg-8(or484)* and *zyg-8(or490)*, which encode proteins mutated in the DCX (G219E) and kinase (G491E) domains, respectively (Gonczy et al., 2001). Although we cannot formally preclude neomorphic actions of these mutations, we believe this is unlikely, i.e. the two alleles rather reflect loss-of-function of *zyg-8* because i) in early embryos, *zyg-8(or484)* and *zyg-8(or490)* display phenotypes indistinguishable from those of genetically null alleles (Gonczy et al., 2001), and ii) in fully developed animals, the two mutations result in similar defects (this study).

We used temperature-shift experiments to investigate the contribution of *zyg-8* to embryonic survival (Materials and Methods and Fig. S1). This analysis revealed that *zyg-8* function is required after the first division for full embryonic viability but not beyond gastrulation (Fig. S1C). Thus, *zyg-8* may control most, if not all of the mitotic divisions during the first hours of development, but appears to be dispensable for subsequent mitoses. Mitosis may not be the only function for *zyg-8* since it is expressed throughout development and persists in several post-mitotic tissues in adult animals (see below). To study these functions, we prepared *zyg-8* mutant adults derived from the eggs of *zyg-8(or484)* or *zyg-8(or490)* parents shifted to 25°C after the completion of gastrulation at the permissive temperature.

### ***zyg-8* is expressed by neuronal and non neuronal cells**

To determine where *zyg-8* functions in adult animals, we analyzed the expression pattern of a *P<sub>zyg-8</sub>::YFP* transcriptional fusion that encompasses 2 kb of the 5' regulatory region of *zyg-8* (Materials and Methods). The progeny of injected animals displayed YFP expression in both neuronal and non-neuronal structures, from late embryonic stages to adulthood. Post-embryonic neurons include a few unidentified cells clustered near the nerve ring, some of them projecting dendrites anteriorly like amphid neurons (Fig. 1A1, star and red arrowhead, respectively), numerous motoneurons in the ventral nerve cord (Fig. 1A1, white

arrowheads) and, most obviously the six touch receptor neurons (TRNs): ALML/R, PLML/R, AVM and PVM (Fig. 1A1, 2, yellow arrowheads). The TRNs sense slight mechanical stimuli applied to the cuticle and transduce them into electrical currents for proper locomotory responses (Chalfie, 2009). In addition, the biolistic integration of our reporter construct led to the expression of YFP in the germline (Fig. 1A3), which was expected, from both genetic and molecular data (Gonczy et al., 2001), as well as in hypodermal cells (Fig. 1A4). The latter expression pattern was unexpected considering that other known *DCDC* genes act in neurons, but two distinct *Pzyg-8-ZYG-8::YFP* translational fusion reporters (Materials and Methods) displayed the same profile (data not shown).

To determine where *ZYG-8* accumulates in the animal and confirm the TRN expression, we performed immunolocalization studies, using affinity-purified *ZYG-8* antibodies, together with anti-acetylated tubulin (AcTub) monoclonal antibodies that preferentially decorate TRN processes (Fukushige et al., 1999). As shown in Fig. 1B, *ZYG-8* colocalized with AcTub, indicating that *ZYG-8* is present in touch cells and distributed along the length of their neurites. Anti-*ZYG-8* antibodies also marked the gonad and other structures that include ventral nerve cords (data not shown).

Thus, in addition to its expected germline expression, *zyg-8* is transcribed in hypodermal and neural tissues. Consistent with a role for *zyg-8* in hypodermis function, mutant animals were slightly shorter than wild-type adults (the Dumpy or *Dpy* phenotype) and some animals displayed a roller (*Rol*) phenotype in which animals twist around their antero-posterior axis while crawling (data not shown). Below, we focus on characterizing the neuronal functions of *zyg-8*.

### ***zyg-8* function is required in adults for proper locomotion and touch sensitivity**

We observed that *zyg-8* mutant animals were lethargic (Fig. 2A), a phenotype that has been linked to synaptic defects and is also evident in animals with defects in TRN function (Syntichaki and Tavernarakis, 2004). We used video recordings of wild-type and mutant adults to evaluate the coordination and speed of locomotion. *zyg-8* mutants left sinusoidal tracks in the bacterial lawn indistinguishable from that of wild-type animals and retained their ability to respond to harsh touch. However, they were immobile for long periods of time, displayed reduced speed when moving and, as a consequence, reduced net displacement when compared to wild-type (Fig. 2A). Thus, wild-type *zyg-8* is required for spontaneous motion of adults.

Next, we asked whether *zyg-8* mutant adults also exhibit a touch-insensitive phenotype, using a classical gentle body touch assay (Materials and Methods). When assayed in parallel, *zyg-8* mutant animals were less touch-sensitive than control animals, but more sensitive than *mec-7* beta tubulin mutants (Fig. 2B, compare lanes 1 and 3). Thus, an intact *zyg-8* gene is needed for full touch sensitivity.

We next tested whether this touch-insensitivity phenotype reflects a requirement for *zyg-8* during developing or in mature TRNs. As shown in Fig. 2B (lanes 4-6), shifting young *zyg-8(or484)* adults from 15°C to 25°C led to a severe reduction of their touch response, providing the shift to 25°C was long enough. Similar results were obtained with *zyg-8(or490)* animals and mutant larvae (data not shown). Since TRNs are fully specified and drive a functional mechanotransducing network by the end of the L4 larval stage, this result suggests that *zyg-8* is required for the physiology of fully mature neurons.

### ***zyg-8* controls morphology and growth of *C. elegans* neurons**

MTs are essential for diverse aspects of neuronal biology such as cell division, neurogenesis, migration, vesicular transport, cell shape, polarity and process outgrowth, and guidance (Mollinedo and Gajate, 2003). We thus probed *zyg-8* function further by analyzing the position and morphology of TRNs as well as that of the well-characterized D-type motoneurons. These 19 ventral cord neurons (13 VDs and 6 DDs) express the inhibitory neurotransmitter GABA and extend processes within both the ventral and dorsal nerve bundles of *C. elegans* to perform their function as cross-inhibitors of body-wall muscle contraction (McIntire et al., 1993). Using appropriate GFP markers, we observed significant morphological defects in mutants compared to control animals (Fig. 3 and Tables 1 and 3).

First, although TRN neurons were properly positioned in the vast majority of cases, cell bodies were often misshapen (red arrows in Fig. 3A) and displayed polarity defects, as assessed by the higher rate of monopolar ALM neurons in mutant worms compared to control (~90% vs. 24%, Table 1). Misshapen cell bodies were also noted in mutant D neurons at lower frequency (8% of *or484* and 19% of *or490* mutants). PVM displayed defective ventral projections in 36% of cases in both *zyg-8(or484)* and *zyg-8(or490)* strains (yellow bracket in Fig. 3A), and about 50% of the mutant animals exhibited shortened lateral branches along ALM or PLM neurons (yellow arrows in Fig. 3A), suggesting that in wild-type touch cells, *zyg-8* restricts ectopic process outgrowth.

Second, we observed with high penetrance (up to 100% for PLMs in *zyg-8(or490)* animals) the formation of numerous varicosities along some D-neuron, ALM and PLM

processes (yellow arrowheads in panels B6, A5 and A7). These varicosities are potential indications of transport issues. However, our analysis of the distribution of the mechanotransduction channel subunits MEC-4 and MEC-2, as well as that of the synaptic vesicle marker GFP-RAB-3, does not support the hypothesis of a global disruption of axonal transport in *zyg-8* mutant TRNs (Fig. 4 and Table 2, respectively).

Third, we documented frequent alterations of process growth and wiring in the D neurons, consistent with disorganization of the ventral nerve cord. Seventy-four percent of *zyg-8(or490)* animals displayed defasciculation of D-neurons along the nerve cords, and commissures were missing or extended along the wrong side of the body in 19% of these animals (Table 3). In several *zyg-8* mutant animals, a D axon with SNB-1::GFP clusters that is normally restricted to body wall muscles in wildtype worms, extended into the head region (panel B12, arrows). Many *zyg-8(or484)* and *zyg-8(or490)* mutants exhibited small gaps or thinning in GFP expression along ventral or dorsal nerve cords indicating that some axons failed to extend their full length (panels B7, B10 and B11, compare to B4). Regions of altered expression of the presynaptic vesicle marker *Punc-25-snb-1::GFP* (Hallam and Jin, 1998) were also observed along the dorsal cord of *zyg-8* mutants at 25°C (panels B8 and B9, compare to panel B5). Although outgrowth of the six DD neurons occurs during embryogenesis, DD synapses form *en passant* along the dorsal muscles only at the end of the L1 larval stage. These synapses increase in size by about 30% as the animals grow to their full adult size, and new membrane and synapses are added along the axon (Yeh et al., 2005). Variations in the *snb-1::GFP* expression pattern could be due to abnormal axon morphology, but may also reflect defective transport during axon and synapse growth.

Collectively, these data indicate that an intact *zyg-8* gene is required for neuronal morphology and polarity, restricts ectopic process outgrowth and may also promote axon and synapse growth. Because these aspects of neuronal development are known to depend on MTs, our findings suggest that *zyg-8* has a role in maintaining neuronal MT integrity.

### ***zyg-8* does not affect global protein levels and transport in touch receptor neurons**

Touch receptor neuron MTs are unique within *C. elegans* in at least two respects: they display a larger diameter due to their 15-protofilament architecture (*vs* 11 in the rest of the animal) and they are organized into dense bundles that fill touch cell processes (Chalfie and Thomson, 1979). Since 15-pf MT bundles are required for efficient mechanotransduction (Chalfie, 2009), TRNs constitute an exquisite model system to investigate the structural and physiological role of a MAP on MT dynamics and organization. Fifteen-protofilament MTs

affect touch sensitivity in several ways that include the control of protein levels and the transport of important components of the mechanotransduction machinery (Bounoutas et al., 2009a). We thus investigated the impact of *zyg-8* mutations on protein levels and the distribution of three TRN-specific components: MEC-18, MEC-2 and MEC-4. Antibodies to all three proteins recognized similar amounts of protein in extracts prepared from wild-type and *zyg-8(or484)* animals (Fig. 4A), suggesting that *zyg-8* does not affect protein levels. The cytoplasmic distribution of MEC-18 in mutant TRNs was indistinguishable from that in wild-type cells (data not shown) and MEC-2 and MEC-4 displayed overlapping punctate patterns along TRN processes, with no gross reduction in the size or number of individual puncta (Fig. 4B). Together, these findings indicate that the loss of touch sensitivity in *zyg-8* mutant animals is unlikely to result from altered protein levels or from mislocalization of mechanotransduction channels.

To further probe putative roles of *zyg-8* in axonal transport, we examined the distribution of the synaptic vesicle marker GFP-RAB-3 (Bounoutas et al., 2009b) in mutant TRNs. Our analysis revealed a small increase in defective shape and position of GFP-RAB-3 puncta in the nerve ring compared to controls, and more diffuse GFP and ectopic puncta were observed in both *or484* and *or490* genotypes (Table 2). A four-fold increase in the number of animals with ectopic puncta in PLM processes was also noted for both *zyg-8* alleles (Table 2). These defects are compatible with weak transport and polarity defects, so that not all synaptic vesicles are tightly clustered at synapses. Although they could contribute to the Mec phenotype of *zyg-8* mutant animals, the primary synaptic output of the mechanosensory neurons is via gap junctions, and mutants that exhibit significant defects in differentiation of chemical synapses are not necessarily Mec (Zheng et al., 2011). Moreover, these defects in synaptic vesicle localization do not reflect global transport failure, as assessed by the proper local delivery of MEC-2 and MEC-4 (Fig. 4B).

### ***zyg-8* maintains the integrity, number, length and bundling of 15-pf MTs**

To test whether *zyg-8* promotes MT stabilization and to gain insight in the corresponding mechanism, we compared the phenotypes induced by *zyg-8* loss-of function and treatment with the MT-depolymerizing drug colchicine. As shown in Fig. 5A, *zyg-8* loss-of-function and colchicine displayed distinct morphological phenotypes. Indeed, process varicosities observed on TRN processes of *zyg-8* mutants were never found upon colchicine treatment (compare Fig. 3A7 and 5A1-4 for instance). Instead, we noted a colchicine dose-dependent decrease in the *Pmec-4::GFP* signal, a phenotype never observed in *zyg-8* mutants.

In addition, we observed strong synthetic effects of *zyg-8* loss-of-function and colchicine, both in the morphology (Fig. 5A5-8) and function (Fig. 5B) of TRNs. TRN processes of *zyg-8* mutant animals treated with low doses of colchicine consistently developed numerous ectopic secondary branches (yellow arrows) that could further branch and cell bodies were often jagged, stellate and disconnected from their physiological targets, as illustrated in panel A6 for instance. The functional consequences of those synthetic effects are best evidenced at 0.1 mM colchicine, a drug concentration that reduces body touch response of *zyg-8* mutant animals by 10-fold versus only 2-fold in control animals (Fig. 5B).

Because colchicine affects MT stability by preventing polymerization, the synergistic effects of *zyg-8* loss-of-function and colchicine suggest that *zyg-8* promotes MT stability through mechanisms at least partially distinct from the sole control of polymer dynamics. To gain further insights in such mechanism in TRNs, we proceeded to the ultrastructural analysis of these neurons in *zyg-8* mutant adults. High-pressure frozen (HPF) animals prepared for transmission electron microscopy (Materials and Methods) revealed several microtubule defects in mutant TRNs (Fig. 6). First and most obviously, the average number of MTs that normally fill TRN processes was reduced. On average, there were  $12.6 \pm 3.5$  ( $N = 14$  touch receptor neurons) microtubules per cross-section in *zyg-8* mutants compared to  $25.3 \pm 3.0$  ( $N = 25$  touch receptor neurons) in wild type animals raised at 25°C. Thus, wild-type *zyg-8* is required for the assembly or maintenance of the large MT array that are hallmarks of the TRNs.

Second, we observed in *zyg-8* mutant TRNs, a notable disorganization of MTs that failed to cluster in the regular bundle-like arrays found in wild-type neurons (Fig. 6A1-3). In a geometrical point of view, the level of organization of these structures can be accounted for by the variability of the distance separating adjacent MTs within the array: in principle, a regular bundle has normal (Gaussian) distribution of nearest-neighbor inter-MT distances, while a disorganized bundle will exhibit a non-normal distribution. Consistent with the idea that *zyg-8* is required to properly organize the MT bundle, the distribution of inter-MT distances differ in wild-type and *zyg-8(or484)* mutant TRNs (Fig. 6C). In addition, MTs are closer to each other in *zyg-8* mutant TRNs, as revealed by the median of the distributions: 34.6 nm vs 39.0 nm, respectively. We propose from this analysis that *zyg-8* plays key roles in the establishment or maintenance of the regular, bundled organization of TRN MTs.

Third, the analysis and digital alignment of serial sections encompassing up to 2.4  $\mu\text{m}$  of body length (Materials and Methods) revealed a 5-fold decrease in MT length in TRNs of mutant animals (Fig. 6D): on average, wild-type TRN MTs were  $14.8 \pm 1.4 \mu\text{m}$  long whereas

in *zyg-8(or484)* animals, this length was reduced to  $3.0 \pm 0.4 \mu\text{m}$ . We conclude that, as a MAP, wild-type *zyg-8* is needed to maintain long MTs in TRNs.

Fourth, when looking at high magnifications of individual MT sections, we observed no difference in protofilament content between *zyg-8* mutant and wild-type animals (Fig. 6A4-6), indicating that, in the context of TRNs, the *DCDC* gene *zyg-8* is dispensable for the assembly or maintenance of 15-pf MTs. However, we also noticed on the same images, a slight but significant reduction of MT caliber in mutant TRNs, as well as a lower signal-to-noise ratio that hinders the sharp resolution of individual protofilaments displayed on wild-type sections (compare Fig. 6A4 to 6A5-6 and Fig. 6E). The gene may also be dispensable for regulating the protofilament content of the 11-pf MTs found in other neurons, including those in the ventral nerve cord (Fig. S2).

Altogether, our ultrastructural analysis establishes that, in TRNs, wild-type ZYG-8 is needed to promote the integrity of the 15-pf MT array through the maintenance of MT number, MT length and MT bundling. The gene is dispensable for the control of pf content *in vivo* although it may still contribute to the structural integrity of individual MTs.

## Discussion

### ***zyg-8* physiology at a whole organism scale**

We show here that *zyg-8* is expressed in *C. elegans*, in post-mitotic neurons where it contributes to most of the functions attributed to *DCDC* genes in mammals, including cellular morphology, axon outgrowth and guidance as well as synaptic vesicle localization. These functions may reflect underlying roles of the gene in the establishment or maintenance of neuronal polarity. Additional phenotypic and genetic analyses will be necessary to determine if there are signaling pathways connecting *zyg-8* directly to the polarity machinery, or if these phenotypes are secondary to functions of *zyg-8* in MT dynamics, stabilization or bundling. However, our findings indicate that the pleiotropic functions of *DCDC* genes in the cortex of mammals are likely to be of ancient origin rather than resulting from recent sub-specialization of these MAPs upon cerebrocortical tissue compartmentalization.

In addition to these functions that may rely on intrinsic properties of the DCX domain, our study reveals an unanticipated role for *zyg-8* in mechanosensation. A recent study in fly sensory cilia showed that the *Drosophila* *DCDC* protein DmELP-1 is implicated in mechanotransduction (Bechstet et al., 2010). DmELP-1 is a multidomain protein containing both a DCX domain and a domain related to the Echinoderm Microtubule-Associated Protein (EMAP) family of proteins. It is not known whether the contribution of DmELP-1 to mechanotransduction is conferred by its DCX or EMAP-like domains. Because the *C. elegans* EMAP, CeELP-1, is expressed in TRNs and is required for touch sensation (Hueston et al., 2008), it may be concluded from these two studies that EMAP-like proteins display conserved function in mechanosensation in a way that might not involve the DCX domain. Our work suggests that the DCX domain displays the ability to stabilize MT-based mechanosensors. In this context, it would be interesting to test whether ZYG-8 and CeELP-1 functionally cooperate in touch neurons and recapitulate the activity of DmELP-1 in mechanotransduction. The stabilizing function of *DCDC* proteins on large MT-based structures may not be restricted to invertebrate cells, as a recent report established the functional association of *DCDC2* with primary cilia in rat hippocampal neurons (Massinen et al., 2011). The presence in the inner ear of mammals of specialized cells filled with complex MT structures that display both unusual architecture and extensive bundling and that are essential to the conversion of sounds into electrical currents, should stimulate closer inspection of the expression of *DCDC* genes in this tissue (Tolomeo and Holley, 1997).

Most eukaryotic mechanotransducing systems involve large cytoskeletal structures that are thought to constitute a rigid support towards mechanical deformations and contribute to gating transducing ion channels (Syntichaki and Tavernarakis, 2004). Both microtubule internal architecture and intermolecular organization such as their bundling may affect the mechanical properties of these structures, by a direct effect on the intrinsic rigidity of the polymer or by an increase of the overall stiffness of the system (Tolomeo and Holley, 1997). However, MT architecture and MT bundling are often intimately linked, so that defining the relative contribution of these two levels of MT organization in mechanosensitive responses is not an easy task. *Caenorhabditis elegans* TRNs represent a useful model system to tackle this issue because the 15-pf MT bundles that fill their processes are unique within the animal and their physiological requirement is genetically tractable. (In nematodes, ordinary MTs are built from 11 pfs and are not clustered in bundles). Chalfie and colleagues demonstrated that 15-pf MT bundles play specific role in mechanosensation, in part by insuring normal protein levels of components of the transduction machinery and transport of mechanosensory channel subunits along the TRN processes (Bounoutas et al., 2009a). However, because 11-pf MTs do not form bundles, no conclusion could be drawn regarding the physiological relevance of MT architecture and MT bundling.

Here we show that *zyg-8* is needed for full mechanosensation, with no impact on protein levels or axonal transport in TRNs, suggesting that the gene plays rather direct roles in the process. Our findings also show that MT architecture and MT bundling are submitted to separate regulatory controls. Indeed, *zyg-8* mutant animals display disorganized TRN MT bundles, with fewer and shorter MTs, but no disruption of the 15-pf MT architecture. Therefore, it could be concluded that maintaining 15-pf MTs in *C. elegans* TRNs is not sufficient, *per se*, to ensure proper mechanosensation and that MT bundling plays crucial role in that process. Although we do not have the ability to measure the stiffness of TRN MT bundles, our findings are compatible with a scenario in which both the 15-pf MT architecture and MT bundling contribute to the rigidity of the array, which, in turn, defines the level of responsiveness of the system.

Our reporter gene analysis suggests that *zyg-8* is somatically transcribed in non-neuronal tissues such as the hypodermis. Although the presence of the ZYG-8 protein remains to be demonstrated in these cells, the Rol and Dpy phenotypes of *zyg-8* mutant animals are compatible with a role of the gene in that tissue. The *C. elegans* hypodermis performs many functions during early development, including establishing the basic body plan, depositing basement membrane components, regulating cell fate specification of neighboring cells,

guiding cell and axon migrations, and taking up apoptotic cell bodies by phagocytosis (Altun and Hall, 2009). Microtubules are likely to participate to most of these developmental processes but to date, their physiological control has not been thoroughly investigated in this tissue. Interestingly, in mammals, individual cells of the olfactory epithelium also express *DCX* and *DCLKs* (Reiner et al., 2006), suggesting a possible ancestral function of these genes in epithelia formation. More work will be necessary to shed light on putative non neuronal functions of *DCDC* genes, but *C. elegans* and *zyg-8* will undoubtedly be instrumental in such a quest.

### **Neuronal *zyg-8* functions as a MT stabilizer and organizer**

The ultrastructural study that we performed allowed us to precisely and quantitatively describe the MT stabilizing role of *zyg-8*, in the physiological context of a developing organism. We show that the gene controls MT number, MT bundling, MT length, but with no associated modification of pf number. One may ask whether these activities are interdependent or rather involve distinct properties of ZYG-8. MT bundling and number may be governed by independent processes, as we consistently find organized MTs in wild-type TRNs, even in the ones that contain less than 10 MTs (data not shown). Conversely, we hardly find well-organized MT bundles in the TRNs of *zyg-8* mutant animals, even in those displaying 20-40 MTs (data not shown).

In *zyg-8(or484)* mutant animals, the average MT content of TRNs is reduced by nearly two-fold and MTs are, on average, five-fold shorter than their wild-type counterparts. This suggests that *zyg-8* displays important stabilizing and/or nucleating functions in TRNs. In one-cell stage *C. elegans* embryos, *zyg-8* also affects spindle MT growth and nucleation and loss of its function can be phenocopied by the MT-depolymerizing drug nocodazole (Gonczy et al., 2001; Srayko et al., 2005). Therefore, *zyg-8* may display similar regulatory activities towards MTs *in vivo*, both in mitotic and post-mitotic contexts.

One of the most striking defects of *zyg-8* mutant TRNs is the disorganization of MTs that fail to cluster as a regular bundle. Consistent with this idea, inter-MT distance varies much more in mutant TRNs than wild-type neurons. In addition, MTs are closer to each other in mutant cells, indicating that ZYG-8 is unlikely to hold bundled MTs together. Our data are more compatible with a model in which ZYG-8 controls the regular spacing between adjacent MTs. Doublecortin-domain containing proteins, including ZYG-8, are usually considered as MT bundling factors, based on their ability to elicit these large MT structures when expressed in cultured cells, but our analysis suggests that more subtle functions of these proteins may be

unravelling in systems where MT bundles constitute the physiological state, such as *C. elegans* TRNs (Coquelle et al., 2006; Gonczy et al., 2001).

Moore and colleagues have dissected the mechanism of MT stabilization by human DCX (Moore et al., 2004; Moore et al., 2006). Notably, they established that DCX selectively promotes the assembly of 13-pf MTs (the major MT architecture in mammals) and stabilizes this architecture *in vitro*. This would result from the unique binding site of DCX in between pfs, where it would ideally control inter-pf lateral contacts and constrain pf number within MTs. DCX may also stabilize longitudinal interactions along pfs in addition to stapling them laterally (Fourniol et al., 2010). This would account for the potent anti-catastrophe and nucleation activities of DCX towards mammalian MTs *in vitro*, and, by extension, predict similar behaviors of DCDC proteins in various systems. However, the model does not predict the architectural properties of endogenous DCDCs in physiological systems deprived of 13-pf MTs. Do they retain and adapt their stapling function to MT architectures with less or more than 13 pfs or is this activity governed by the geometry of 13-pf MTs? In this context, *C. elegans* constitutes a model of choice because its cells are filled with either 11 pf-MTs or 15-pf MTs. Our findings that a DCDC protein is expressed in *C. elegans* TRNs and other neurons indicates that the DCX domain *per se* is not sufficient to constrain any type of MT to adopt the 13-pf architecture *in vivo*. Because *zyg-8* function is dispensable to the assembly or maintenance of both types of MT architectures in worms, it may be concluded that the stapling model proposed by Moore and colleagues may not apply to all DCDC proteins or is restricted to 13-pf MTs. While it has been suggested in the literature that 15-pf MTs are the result of specific alpha and beta tubulins (Chalfie and Thomson, 1982), respectively MEC-12 and MEC-7, these isoforms are not exclusive to the TRNs. Potential alternative mechanisms include both other MAPs and post-translational modifications like  $\alpha$ -tubulin acetylation, recently shown to be needed for the formation of uniform bundles of 15-pf microtubules in *C. elegans* touch receptor neurons (Cueva et al., 2012; Topalidou et al., 2012). *zyg-8* has no paralog in *C. elegans* genome but two unrelated MAPs, PTL-1 and ELP-1, have been shown to be expressed in TRNs and required for mechanosensation (Gordon et al., 2008; Hueston et al., 2008). Although the role of these proteins on MT architecture remains to be demonstrated, they represent interesting candidates to supply *zyg-8* loss-of-function.

Despite the lack of a strict requirement for *zyg-8* in the maintenance of TRN MT architecture, we measure a slight but significant decrease of MT diameter in mutant animals, associated to less defined protofilaments when compared to wild-type. Because the animals have been grown, fixed and processed for TEM analysis the same way in the same conditions,

we believe these subtle defects may reflect cryptic alterations of the structure. Taken together, our ultrastructural findings demonstrate that an intact *zyg-8* gene acts to maintain MT length, number and organization in TRNs.

## Materials and Methods

### Nematode strains and transgenesis

*C. elegans* (N2) culture was performed according to standard methods (Brenner, 1974). *zyg-8* mutant alleles were described previously (Gonczy et al., 2001). In the course of this study, we outcrossed the two *zyg-8*ts alleles *zyg-8(or484)* and *zyg-8(490)* from their original *lin-2* background, through conventional genetic crosses. The resulting strains were subsequently crossed with SK4005 *zDis5 (Pmec-4::GFP)*, NM2689 *jsIs821 (Pmec-7::GFP-RAB-3)* (Bounoutas et al., 2009b), CZ333 *juIs1 (Punc-25::GFP-SNB-1)* (Zhen and Jin, 1999), *juIs145 (Pflp-13::GFP)* (Sakaguchi-Nakashima et al., 2007), and CZ1200 *juIs76 (Punc-25::GFP)* (Huang et al., 2003) integrated transgenic lines to examine, respectively, touch receptor neurons or D-type motoneuron morphology upon *zyg-8* loss-of-function. The CB1477 *mec-7(e1343)X* strain (Savage et al., 1989) was used as positive control in gentle body touch assays.

Transgenesis was performed by conventional microinjection methods (Mello et al., 1991) and by biolistic bombardment on a Bio-RadPDS-1000/He Hepta System, following previously reported procedures (Praitis et al., 2001) optimized by C. Canard (P. Gönczy lab).

### Constructs and *zyg-8* promoter validation

The YFP reporter construct *Pzyg-8::YFP* was engineered by subcloning 2 kb of genomic DNA sequence located immediately upstream of the predicted +1 codon of *zyg-8* in the BamH I/Nhe I sites of the Addgene plasmid 1662. This construct was subsequently used as a backbone to insert the *zyg-8* full-length cDNA sequence at the Nhe I/Kpn I sites and thus generate *Pzyg-8-zyg-8c::YFP*. We also created the intron 1-containing *Pzyg-8-zyg-8g::YFP* construct by replacing the 1.65 kb Bgl II/Pas I fragment from *Pzyg-8-zyg-8c::YFP* by the corresponding *zyg-8* genomic sequence. All these constructs have been verified by sequencing. In addition, we made use of the previously described *Ppie1::GFP-zyg-8* plasmid, that has been shown to partially rescue the Maternal-effect Embryonic Lethality (MEL) of non-conditional, balanced, *unc-32(e189) zyg-8(t1650)* homozygous animals (Gonczy et al., 2001).

The four constructs, upon biolistic bombardment, line selection and western-blot extract analyses, encoded proteins with the expected sizes that displayed epitopes for anti-GFP or anti-ZYG-8 antibodies (data not shown). Furthermore, when crossed with the *unc-32(e189) zyg-8(t1650)* strain, *Pzyg-8-zyg-8g::YFP* (as well as *Ppie1::GFP-zyg-8*)

resulted in the segregation of living (Unc) progeny from *zyg-8* homozygous Unc F2 animals (data not shown). This partial rescue of the MEL phenotype of *zyg-8(t1650) -/-* animals biologically validated our 2 kb regulatory sequence as a *bona fide* *zyg-8* promoter sequence.

### **Anti-ZYG-8 antibodies**

For this work, we generated new affinity-purified anti-ZYG-8 antibodies, essentially as described before, with few modifications (Bellanger and Gonczy, 2003). Briefly, the *zyg-8* full-length cDNA was subcloned into a modified pMalC2X prokaryote expression vector and recombinant MBP-ZYG-8 was produced in *E. coli* BL21 cells, as soluble and insoluble (inclusion bodies) fractions. A rabbit was immunized with inclusion bodies while the soluble fraction was cleaved with Factor Xa. Cleaved products (250 µg) were separated by SDS-PAGE, transferred onto nitrocellulose and stained with Ponceau Red to cut a strip that encompassed the ~100 kDa ZYG-8 band. We proceeded to affinity purification by incubating the strip with sera for 2 h at 4°C, then eluting specific antibodies with 0.1 M glycine pH 2.0 before neutralization with 1 M Tris pH 8.0.

### **Temperature-shift experiments**

Temperature-shift experiments and progeny-tests were conducted as described previously (Bellanger et al., 2007). The end of the *zyg-8* Temperature-Sensitive Period (TSP) was determined by collecting embryos at different developmental stages, and measuring their survival rate upon temperature shift. “Early” embryos were collected by dissecting gravid hermaphrodites and thus correspond to 1-30-cell stage embryos approximately. Older embryos were collected as eggs laid over a 10 h period of time (at 15°C). They thus correspond to ~30-400 cell stage embryos. Since (1) only “early” embryos displayed embryonic lethality (Fig. S1C), (2) gastrulation ends 3h (at 25°C) after eggs have been laid and (3) we previously determined that the maternal pool of *zyg-8(or484)* inactivates within 12h following their shift to 25°C, the *zyg-8* TSP likely encompasses most of the gastrulation process.

Larvae and adult animals that hatched from eggs shifted to 25°C after the completion of gastrulation, displayed no or minor developmental defects. We noted slight Dumpy phenotypes and occasional rollers, suggesting a role for *zyg-8* in the metabolism of collagen, beyond the scope of this study.

### **Gentle body touch assay**

Body touch sensitivity of worms was assayed as follows: 20-30 animals/condition were gently touched with an eyebrow hair glued to a toothpick, 5 times to the anterior body, alternately with 5 times to the posterior body. Control animals move backward when touched anteriorly and forward when stroked posteriorly. We scored as positive the animals that responded 5 or 4 times out of the 5 touches. Since we noticed higher variability in the anterior response, we chose not to pool both responses and to present only data corresponding to the posterior body touch sensitivity. Figs. 2B and 5B illustrate the response of adult animals that have been shifted to 25°C as post-gastrulating embryos or adults, as indicated. CB1477 *mec-7* animals and the MT-depolymerizing drug colchicine, were used as genetic and chemical positive controls in Figs. 2B and 5B, respectively (Chalfie and Thomson, 1982).

### **Microscopy**

Locomotion and morphological defects were analyzed on a Leica Z16 APO stereomicroscope. Lethargy was monitored at 25°C by recording adult mutant animals transferred onto fresh plates 15' prior to starting the movies. Movies were 3 min long, 1 image per second. The position of the worm was marked on each frame to reconstruct its track and to extract three parameters: peak velocity "V", averaged velocity "v" and lethargy ratio "L" (defined as the fraction of time of total immobility).

ZYG-8 immunofluorescence and YFP reporter studies were exclusively performed on a Zeiss Axioplan2 / LSM510 Meta confocal microscope, at the Montpellier RIO Imaging facility. Zero.7 to 0.9  $\mu\text{m}$ -thick optical slices were collected and used as such for colocalization studies, or z-stacked to reconstruct the whole animal thickness. Motoneuron GFP reporters were imaged using a Nikon E800 microscope equipped with Photometrics CoolsnapES CCD camera and Metamorph software.

### **Serial-section electron microscopy**

Nematodes were raised at 25°C from hatching and prepared for electron microscopy by high-pressure freezing (HPF) followed by freeze substitution (in 2% glutaraldehyde, 1% osmium tetroxide), as described (Cueva et al., 2007). Following embedding in Eponate 12/Araldite 502, serial, 40-nm sections were cut and collected on Formvar-coated, copper-slot grids. A novel post-staining method, which will be described in detail elsewhere (J. Cueva, M. Goodman, unpublished), was used to enhance contrast and to visualize microtubule protofilaments. Sections were tilted 20°C, imaged on a TEM (JEOL TEM 1230, Tokyo,

Journal of Cell Science • Accepted manuscript

Japan) and digital images were acquired with an 11-megapixel bottom-mounted cooled CCD camera (Orius SC1000, Gatan, Pleasanton, California). Images from serial sections were manually aligned using Reconstruct (Fiala, 2005). Microtubule number was counted by hand and used to calculate MT length, as described (Chalfie and Thomson, 1979). The bundled organization of TRN microtubules was estimated via the distribution of inter-MT distances within a given cell. Indeed, a perfect bundle displays regularly spaced MTs, associated with inter-MT distances that peak around the average value. In contrast, the variable MT-MT spacing that features disorganized MT geometries is predicted to yield a distribution of inter-MT distances more spread along the length axis. In practise and to compensate for the intracellular variability of MT organization along TRN processes, we first selected, in each serial section, 5-6 images distant from a 300-500 nm step. On each image, we drew lines connecting the center of every MT to the center of its immediate neighbors. The length of each line was then determined, collected and plotted as a function of its relative abundance within the whole collection.

### **Indirect immunofluorescence**

Fixation of nematodes for indirect immunofluorescence was performed according to established protocols (Gendrel et al., 2009), with few modifications introduced by M. Gendrel (J.-L. Bessereau lab). Briefly, worms were sandwiched between two SuperFrost Plus glass slides (ThermoScientific) that do not require any coating. The sandwich was then warmed for 5 sec on a hot aluminium block and immediately placed on another block that was sitting on dry ice for 20 min or more. Cuticles were cracked by splitting the two frozen slides apart with a razor blade, and open worms were immediately fixed and permeabilized in 3.2% paraformaldehyde and 0.1% Triton X-100 (ZYG-8 staining) or in cold acetone and methanol (other stainings). After washing, worms were split in as many tubes as intended conditions and further processed to immunostaining. The following primary antibodies were utilized: 1:50 rabbit affinity-purified anti-ZYG-8, 1:500 mouse anti-acetylated Tubulin (6-11B-1, Sigma, kindly provided by C. Janke), 1:100 rabbit anti-MEC-2 (kindly provided by A. Bounoutas, M. Chalfie lab), 1:100 mouse anti-MEC-4 (ab22184, Abcam) and 1:1000 rabbit anti-MEC-18 (kindly provided by A. Bounoutas, M. Chalfie lab). Secondary antibodies were 1:1000 goat anti-mouse conjugated to Alexa-488 and 1:1000 goat anti-rabbit conjugated to Alexa-546 (Molecular Probes).

### **Western-blotting**

Western-blot analysis was performed as described (Bellanger and Gonczy, 2003) using nitrocellulose membranes (Protran, Schleicher & Schuell). Primary antibodies used were: 1:1000 rabbit anti-GFP (Torrey Pines), 1:2000 mouse anti- $\alpha$ Tubulin (DM1 $\alpha$ , Sigma), 1:100 rabbit anti-ZYG-8, 1:500 rabbit anti-MEC-2 (kindly provided by A. Bounoutas, M. Chalfie lab), 1:500 mouse anti-MEC-4 (ab22184, Abcam) and 1:1000 rabbit anti-MEC-18 (kindly provided by A. Bounoutas, M. Chalfie lab). The secondary HRP-coupled anti-mouse and anti-rabbit antibodies were diluted in PBS and utilized at 1:10,000. The ECL reaction was performed as recommended by the manufacturer (Amersham Pharmacia).

## Acknowledgments

We thank Jean-Louis Bessereau, Jérôme Boudeau, Pierre Gönczy, Anne Houdusse, Lionel Pintard and Susanne Schmidt for critical reading of the manuscript, Sylvie Fromont for technical help in molecular biology, Riva DiGiacomo for help in strain construction, Montpellier RIO Imaging for confocal microscopy analyses, the antibody production facility of the CRBM and the *Caenorhabditis* Genetic Center for strains. Work was supported by CNRS institutional grants (AD), NIH NS047715 and EB 006745 (MBG) and NSF 064221 (RB).

## References

- Altun, Z. F. and Hall, D. H.** (2009). Epithelial system, hypodermis. *In WormAtlas*.
- Bechstedt, S., Albert, J. T., Kreil, D. P., Muller-Reichert, T., Gopfert, M. C. and Howard, J.** (2010). A doublecortin containing microtubule-associated protein is implicated in mechanotransduction in *Drosophila* sensory cilia. *Nat Commun* **1**, 11.
- Bellanger, J. M., Carter, J. C., Phillips, J. B., Canard, C., Bowerman, B. and Gonczy, P.** (2007). ZYG-9, TAC-1 and ZYG-8 together ensure correct microtubule function throughout the cell cycle of *C. elegans* embryos. *J Cell Sci* **120**, 2963-73.
- Bellanger, J. M. and Gonczy, P.** (2003). TAC-1 and ZYG-9 form a complex that promotes microtubule assembly in *C. elegans* embryos. *Curr Biol* **13**, 1488-98.
- Bielas, S. L., Serneo, F. F., Chechlacz, M., Deerinck, T. J., Perkins, G. A., Allen, P. B., Ellisman, M. H. and Gleeson, J. G.** (2007). Spinophilin facilitates dephosphorylation of doublecortin by PP1 to mediate microtubule bundling at the axonal wrist. *Cell* **129**, 579-91.
- Bounoutas, A., O'Hagan, R. and Chalfie, M.** (2009a). The multipurpose 15- protofilament microtubules in *C. elegans* have specific roles in mechanosensation. *Curr Biol* **19**, 1362-7.
- Bounoutas, A., Zheng, Q., Nonet, M. L. and Chalfie, M.** (2009b). *mec-15* encodes an F-box protein required for touch receptor neuron mechanosensation, synapse formation and development. *Genetics* **183**, 607-17, 1SI-4SI.
- Brenner, S.** (1974). The genetics of *Caenorhabditis elegans*. *Genetics* **77**, 71-94.
- Chalfie, M.** (2009). Neurosensory mechanotransduction. *Nat Rev Mol Cell Biol* **10**, 44-52.
- Chalfie, M. and Thomson, J. N.** (1979). Organization of neuronal microtubules in the nematode *Caenorhabditis elegans*. *J Cell Biol* **82**, 278-89.
- Chalfie, M. and Thomson, J. N.** (1982). Structural and functional diversity in the neuronal microtubules of *Caenorhabditis elegans*. *J Cell Biol* **93**, 15-23.
- Coquelle, F. M., Levy, T., Bergmann, S., Wolf, S. G., Bar-El, D., Sapir, T., Brody, Y., Orr, I., Barkai, N., Eichele, G. et al.** (2006). Common and divergent roles for members of the mouse DCX superfamily. *Cell Cycle* **5**, 976-83.
- Cueva, J. G., Hsin, J., Huang, K., C. and Goodman, M. B.** (2012). Posttranslational acetylation of  $\alpha$ -tubulin constrains protofilament number in native microtubules. *Curr Biol* (epub ahead of print).
- Cueva, J. G., Mulholland, A. and Goodman, M. B.** (2007). Nanoscale organization of the MEC-4 DEG/ENaC sensory mechanotransduction channel in *Caenorhabditis elegans* touch receptor neurons. *J Neurosci* **27**, 14089-98.
- Deuel, T. A., Liu, J. S., Corbo, J. C., Yoo, S. Y., Rorke-Adams, L. B. and Walsh, C. A.** (2006). Genetic interactions between doublecortin and doublecortin-like kinase in neuronal migration and axon outgrowth. *Neuron* **49**, 41-53.
- Edelman, A. M., Kim, W. Y., Higgins, D., Goldstein, E. G., Oberdoerster, M. and Sigurdson, W.** (2005). Doublecortin kinase-2, a novel doublecortin-related protein kinase associated with terminal segments of axons and dendrites. *J Biol Chem* **280**, 8531-43.
- Fiala, J. C.** (2005). Reconstruct: a free editor for serial section microscopy. *J Microsc* **218**, 52-61.
- Fourniol, F. J., Sindelar, C. V., Amigues, B., Clare, D. K., Thomas, G., Perderiset, M., Francis, F., Houdusse, A. and Moores, C. A.** (2010). Template-free 13-protofilament microtubule-MAP assembly visualized at 8 Å resolution. *J Cell Biol* **191**, 463-70.
- Fukushige, T., Siddiqui, Z. K., Chou, M., Culotti, J. G., Gogonea, C. B., Siddiqui, S. S. and Hamelin, M.** (1999). MEC-12, an alpha-tubulin required for touch sensitivity in *C. elegans*. *J Cell Sci* **112** ( Pt 3), 395-403.

**Gendrel, M., Rapti, G., Richmond, J. E. and Bessereau, J. L.** (2009). A secreted complement-control-related protein ensures acetylcholine receptor clustering. *Nature* **461**, 992-6.

**Gonczy, P., Bellanger, J. M., Kirkham, M., Pozniakowski, A., Baumer, K., Phillips, J. B. and Hyman, A. A.** (2001). *zyg-8*, a gene required for spindle positioning in *C. elegans*, encodes a doublecortin-related kinase that promotes microtubule assembly. *Dev Cell* **1**, 363-75.

**Gordon, P., Hingula, L., Krasny, M. L., Swienkowski, J. L., Pokrywka, N. J. and Raley-Susman, K. M.** (2008). The invertebrate microtubule-associated protein PTL-1 functions in mechanosensation and development in *Caenorhabditis elegans*. *Dev Genes Evol* **218**, 541-51.

**Hallam, S. J. and Jin, Y.** (1998). *lin-14* regulates the timing of synaptic remodelling in *Caenorhabditis elegans*. *Nature* **395**, 78-82.

**Huang, X., Huang, P., Robinson, M. K., Stern, M. J. and Jin, Y.** (2003). UNC-71, a disintegrin and metalloprotease (ADAM) protein, regulates motor axon guidance and sex myoblast migration in *C. elegans*. *Development* **130**, 3147-61.

**Hueston, J. L., Herren, G. P., Cueva, J. G., Buechner, M., Lundquist, E. A., Goodman, M. B. and Suprenant, K. A.** (2008). The *C. elegans* EMAP-like protein, ELP-1 is required for touch sensation and associates with microtubules and adhesion complexes. *BMC Dev Biol* **8**, 110.

**Koizumi, H., Tanaka, T. and Gleeson, J. G.** (2006). Doublecortin-like kinase functions with doublecortin to mediate fiber tract decussation and neuronal migration. *Neuron* **49**, 55-66.

**Massinen, S., Hokkanen, M. E., Matsson, H., Tammimies, K., Tapia-Paez, I., Dahlstrom-Heuser, V., Kuja-Panula, J., Burghoorn, J., Jeppsson, K. E., Swoboda, P. et al.** (2011). Increased expression of the dyslexia candidate gene DCDC2 affects length and signaling of primary cilia in neurons. *PLoS One* **6**, e20580.

**McIntire, S. L., Jorgensen, E. and Horvitz, H. R.** (1993). Genes required for GABA function in *Caenorhabditis elegans*. *Nature* **364**, 334-7.

**Mello, C. C., Kramer, J. M., Stinchcomb, D. and Ambros, V.** (1991). Efficient gene transfer in *C. elegans*: extrachromosomal maintenance and integration of transforming sequences. *Embo J* **10**, 3959-70.

**Mollinedo, F. and Gajate, C.** (2003). Microtubules, microtubule-interfering agents and apoptosis. *Apoptosis* **8**, 413-50.

**Moores, C. A., Perderiset, M., Francis, F., Chelly, J., Houdusse, A. and Milligan, R. A.** (2004). Mechanism of microtubule stabilization by doublecortin. *Mol Cell* **14**, 833-9.

**Moores, C. A., Perderiset, M., Kappeler, C., Kain, S., Drummond, D., Perkins, S. J., Chelly, J., Cross, R., Houdusse, A. and Francis, F.** (2006). Distinct roles of doublecortin modulating the microtubule cytoskeleton. *Embo J* **25**, 4448-57.

**Praitis, V., Casey, E., Collar, D. and Austin, J.** (2001). Creation of low-copy integrated transgenic lines in *Caenorhabditis elegans*. *Genetics* **157**, 1217-26.

**Pramparo, T., Youn, Y. H., Yingling, J., Hirotsune, S. and Wynshaw-Boris, A.** (2010). Novel embryonic neuronal migration and proliferation defects in *Dcx* mutant mice are exacerbated by *Lis1* reduction. *J Neurosci* **30**, 3002-12.

**Sakaguchi-Nakashima, A., Meir, J. Y., Jin, Y., Matsumoto, K. and Hisamoto, N.** (2007). LRK-1, a *C. elegans* PARK8-related kinase, regulates axonal-dendritic polarity of SV proteins. *Curr Biol* **17**, 592-8.

**Savage, C., Hamelin, M., Culotti, J. G., Coulson, A., Albertson, D. G. and Chalfie, M.** (1989). *mec-7* is a beta-tubulin gene required for the production of 15-protofilament microtubules in *Caenorhabditis elegans*. *Genes Dev* **3**, 870-81.

- Shu, T., Tseng, H. C., Sapir, T., Stern, P., Zhou, Y., Sanada, K., Fischer, A., Coquelle, F. M., Reiner, O. and Tsai, L. H.** (2006). Doublecortin-like kinase controls neurogenesis by regulating mitotic spindles and M phase progression. *Neuron* **49**, 25-39.
- Srayko, M., Kaya, A., Stamford, J. and Hyman, A. A.** (2005). Identification and characterization of factors required for microtubule growth and nucleation in the early *C. elegans* embryo. *Dev Cell* **9**, 223-36.
- Syntichaki, P. and Tavernarakis, N.** (2004). Genetic models of mechanotransduction: the nematode *Caenorhabditis elegans*. *Physiol Rev* **84**, 1097-153.
- Tolomeo, J. A. and Holley, M. C.** (1997). Mechanics of microtubule bundles in pillar cells from the inner ear. *Biophys J* **73**, 2241-7.
- Topalidou, I., Keller, C., Kalebic, N., Nguyen, K. C., Somhegyi, H., Politi, K. A., Heppenstall, P., Hall, D. H. and Chalfie, M.** (2012). Genetically Separable Functions of the MEC-17 Tubulin Acetyltransferase Affect Microtubule Organization. *Curr Biol* (epub ahead of print).
- Wood, W. B., Hecht, R., Carr, S., Vanderslice, R., Wolf, N. and Hirsh, D.** (1980). Parental effects and phenotypic characterization of mutations that affect early development in *Caenorhabditis elegans*. *Dev Biol* **74**, 446-69.
- Yeh, E., Kawano, T., Weimer, R. M., Bessereau, J. L. and Zhen, M.** (2005). Identification of genes involved in synaptogenesis using a fluorescent active zone marker in *Caenorhabditis elegans*. *J Neurosci* **25**, 3833-41.
- Zhen, M. and Jin, Y.** (1999). The liprin protein SYD-2 regulates the differentiation of presynaptic termini in *C. elegans*. *Nature* **401**, 371-5.
- Zheng, Q., Schaefer, A. M. and Nonet, M. L.** (2011). Regulation of *C. elegans* presynaptic differentiation and neurite branching via a novel signaling pathway initiated by SAM-10. *Development* **138**, 87-96.

## Figure legends

### Figure 1: *zyg-8* is expressed in *C. elegans* neurons

(A) Confocal microscopy imaging of *Pzyg-8::YFP* transgenic animals generated by classical microinjection (1 & 2) or biolistic bombardment (3 & 4). Yellow arrowheads point to Touch Receptor Neurons, white arrowheads to motoneurons along the Ventral Nerve Cord, red arrowhead to anterior projections of unidentified head neurons marked by a white star.

(B) Confocal microscopy images of 3 fixed N2 adult animals immunostained with affinity-purified anti-ZYG-8 rabbit antibodies (upper panels), monoclonal 6-11B-1 antibodies that specifically recognize acetylated tubulin (AcTub, middle panels). Lower panels correspond to the merged images (ZYG-8 in red, AcTub in green, colocalization in yellow).

### Figure 2: *zyg-8ts* mutant animals are lethargic and touch insensitive

(A) Still image from representative movies (3 min long, 1 image/sec) of adult animals with the indicated genotypes (N2: wild-type). The position of the tip of each animal recorded over 180 frames and is overlaid in blue on each panel. Peak velocity (V), average velocity (v) and lethargy ratio (L, corresponding to the fraction of time of total immobility during the 3 min recording) have been indicated for each animal. Note the sinusoidal traces left in the bacterial lawn by mutant animals, which reflect their normal coordination. Similar results were obtained for at least 35 animals per genotype.

(B) Touch sensitivity of wild-type and *zyg-8* mutant animals shifted to 25°C as embryos or adults. At least 20 animals were tested for each condition, except for lane 6 in which 13 animals were tested. Note that mutants are less touch sensitive at 15°C and that a 20h-long temperature shift has no effect (lanes 4 and 5).

### Figure 3: *zyg-8* controls various aspects of neuronal morphology in *C. elegans*

(A) TRNs visualized in live animals expressing *Pmec-4::GFP*. (1) DIC-GFP composed image of an adult animal, highlighting positions and projections of the 6 touch cells.

(2-10) Confocal microscopy imaging of representative TRNs from wild-type (2-4, ctr) and *zyg-8(or484)* animals (5-10, *zyg-8*). Panels 2, 5 and 8 illustrate ALM (plus one AVM in panel 2) neurons, panels 3, 6 and 9 PVM neurons, panels 4, 7 and 10 PLM neurons. Yellow arrowheads point to varicosities, yellow arrows to ectopic process outgrowth, red arrows to misshaped cell bodies, and the horizontal bracket marks trajectory defect. A quantification of these defects is provided in Table 1.

(B) D-type motoneuron morphology visualized with *Punc-25::GFP* or *Pflp13::GFP* transgenes and D neuron synapses visualized with the presynaptic vesicle marker *Punc-25-snb-1::GFP*. (1) GFP image showing positions and projections of the 13 VD and 6 DD motoneurons in young adult animals, and (2) diagram of the morphology of a single DD motoneuron with synapses along dorsal muscles. (3-12) Representative D neurons from wild-type (3-5, ctr) and *zyg-8* mutant animals (6-12, *zyg-8*). Projections of wild-type D-type motoneurons in the dorsal nerve cord (3) and D-type neuron cell bodies and processes along the ventral nerve cord (4) are shown. Varicosities (yellow arrows, see text for details) and thinning (yellow bracket) along the dorsal cord of *zyg-8(or484)* animals are depicted in panel 6, and axon fasciculation and morphology defects (red arrows) in the ventral nerve cord of *zyg-8(or490)* worms are illustrated in panel 7. Dorsal synapses of the DD neurons are visualized by SNB-1::GFP expression in wild-type (5) and *zyg-8(or490)* animals (8 and 9). Additional defects observed in *zyg-8(or484)* mutants include DD migration defects (10) and ectopic synapses formed by a misplaced VD axon in the nose/head (12). Panel 11 depicts a newly hatched *zyg-8(or484)* L1 larvae in which the DD neurons extend normally along the dorsal cord, but each cell lacks a posterior dendrite along the ventral cord. A quantification of these defects is provided in Table 3.

In this figure and the following ones, anterior is on the left side and the position of the vulva is marked by a white asterisk.

#### **Figure 4: *zyg-8* does not regulate protein levels and transport in TRNs**

(A) Western-blot analysis of MEC-18, MEC-4, MEC-2 protein content in extracts prepared from wild-type and *zyg-8(or484)* mutant adult worms. Alpha-Tubulin is used as a loading control and MEC-18 is recognized as a doublet.

(B) Confocal microscopy imaging of TRNs in fixed representative wild-type (left panels) and *zyg-8(or484)* mutant (right panels) adult animals immunostained with affinity-purified anti-MEC-2 (top panels) or anti-MEC-4 (middle panels) polyclonal antibodies. Note on the merge image (lower panels) that MEC-2 (green) and MEC-4 (red) colocalize both in wild-type and mutant worms. Bar : 10  $\mu$ m.

#### **Figure 5: *zyg-8* loss-of-function synergizes with colchicine-elicited MT depolymerization in TRNs**

(A) Confocal microscopy imaging of representative GFP-expressing TRNs from wild-type (1-4, ctr) or *zyg-8(or484)* (5-8, *zyg-8*) adult animals grown on 0.1 mM colchicine. 1 and 6:

AVM, 3 and 5: ALM, 2 and 7: PVM, 4 and 8: PLMs. Yellow arrows point to ectopic process outgrowth/branching, red arrows to misshaped cell bodies, red arrowheads to trajectory defects and red stars mark process arborizations. Compare these images to Fig. 3A5-10 to appreciate the synthetic effects of colchicine and *zyg-8* loss-of-function on TRN morphology. (B) Gentle body touch assay. At least 20 animals were tested under each condition.

**Figure 6: *zyg-8* controls MT stability and organization in TRNs**

(A1-A3) Transmission electron micrographs of cross-sections of a TRN (PLM) with the indicated genotypes. Arrowheads mark the TRN-associated extracellular matrix and arrows mark ordinary (11-pf) MTs found in hypodermal cells. Scale bar is 100 nm.

(A4-A6) High magnification views of four selected MTs for each genotype shown protofilament organization. Note the unaltered 15-pf content of TRN MTs in *zyg-8* mutants when compared to wild-type animals. Scale bar is 25 nm.

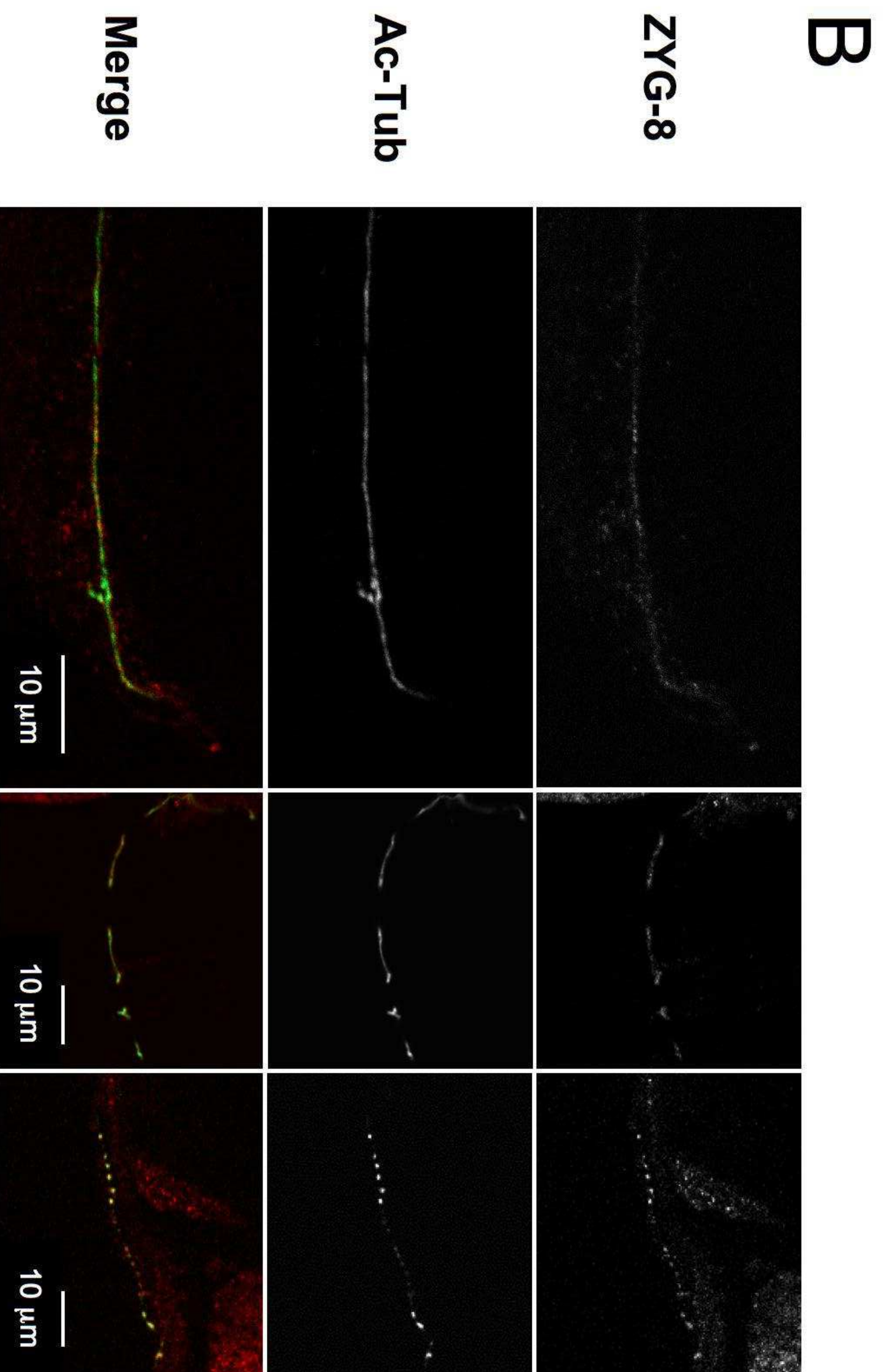
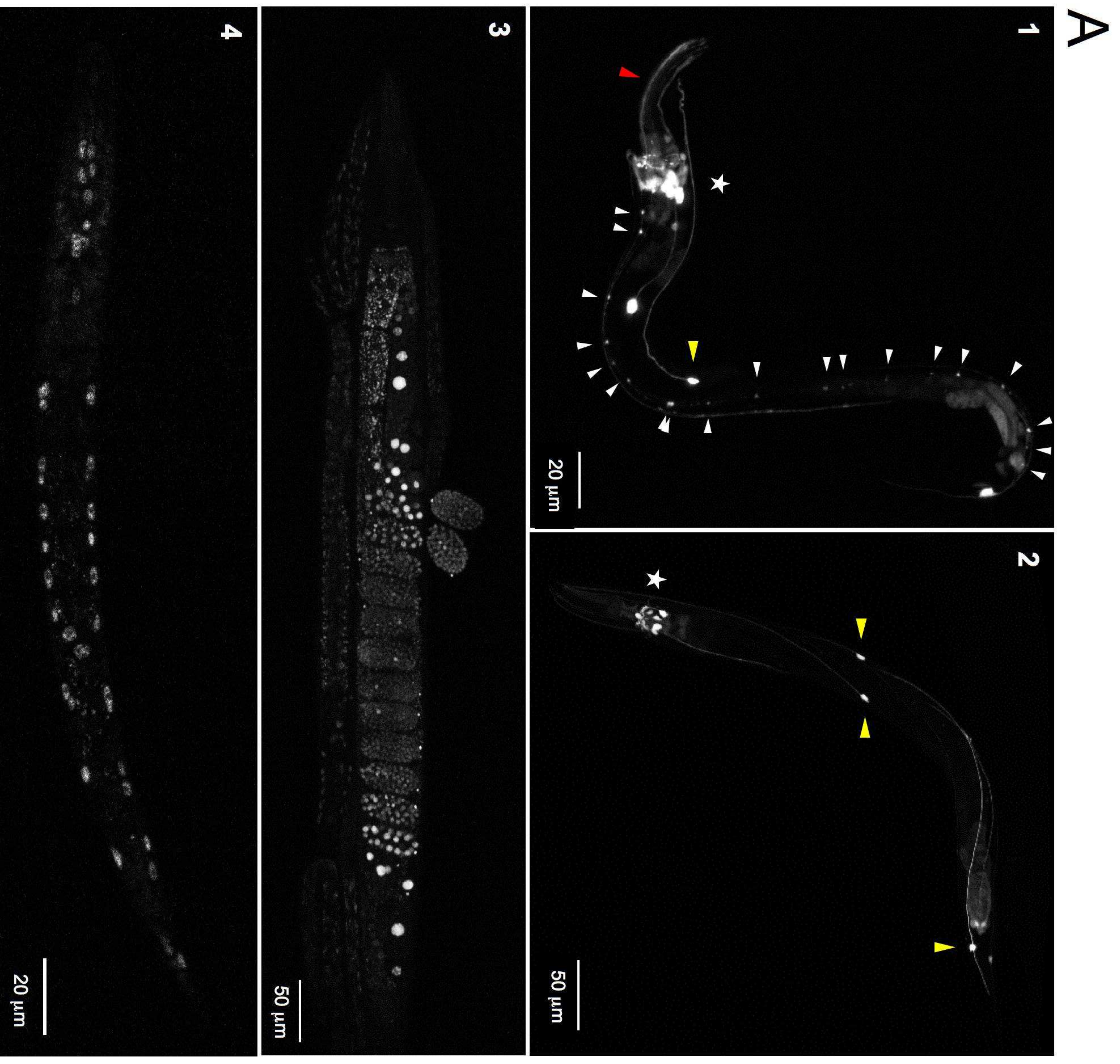
(B) Bar graph representing the average number of MTs per TRN in wild-type and *zyg-8(or484)* animals.

(C) Probability distribution of nearest neighbor inter-MT distances in TRNs of wild-type and *zyg-8(or484)* animals. The median values are indicated by black and blue arrowheads and are 39.0 and 34.6 nm, respectively. The distributions are significantly different ( $p < 0.01$ , KS test).

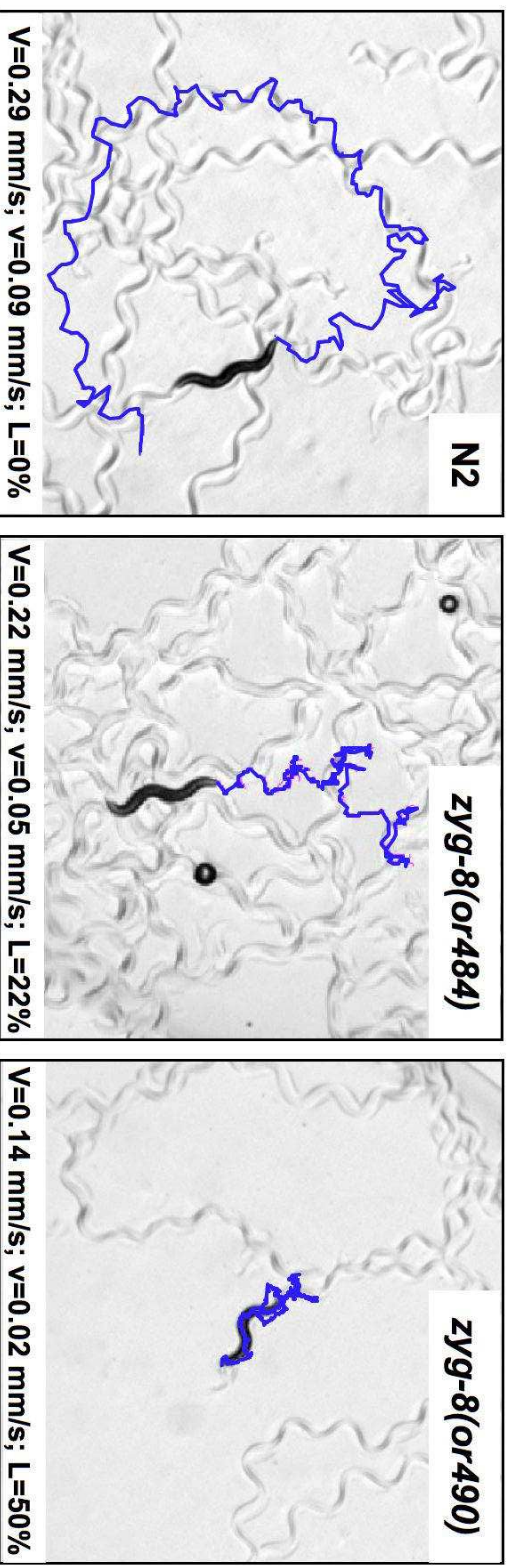
(D) Bar graph representing the average microtubule length per TRNs of wild-type and *zyg-8(or484)* animals, as determined from serial section datasets and digital alignment (Materials and Methods).

(E) Bar graph representing the average diameter of MTs per TRN in wild-type and *zyg-8(or484)* animals.

Asterisks indicate Student Test statistical significance (\* :  $p < 0.01$ ). N = Number of TRNs scored, n = number of individual MTs (panel E) or MT-MT distances (panel C) scored.

**Figure 1**

A



B

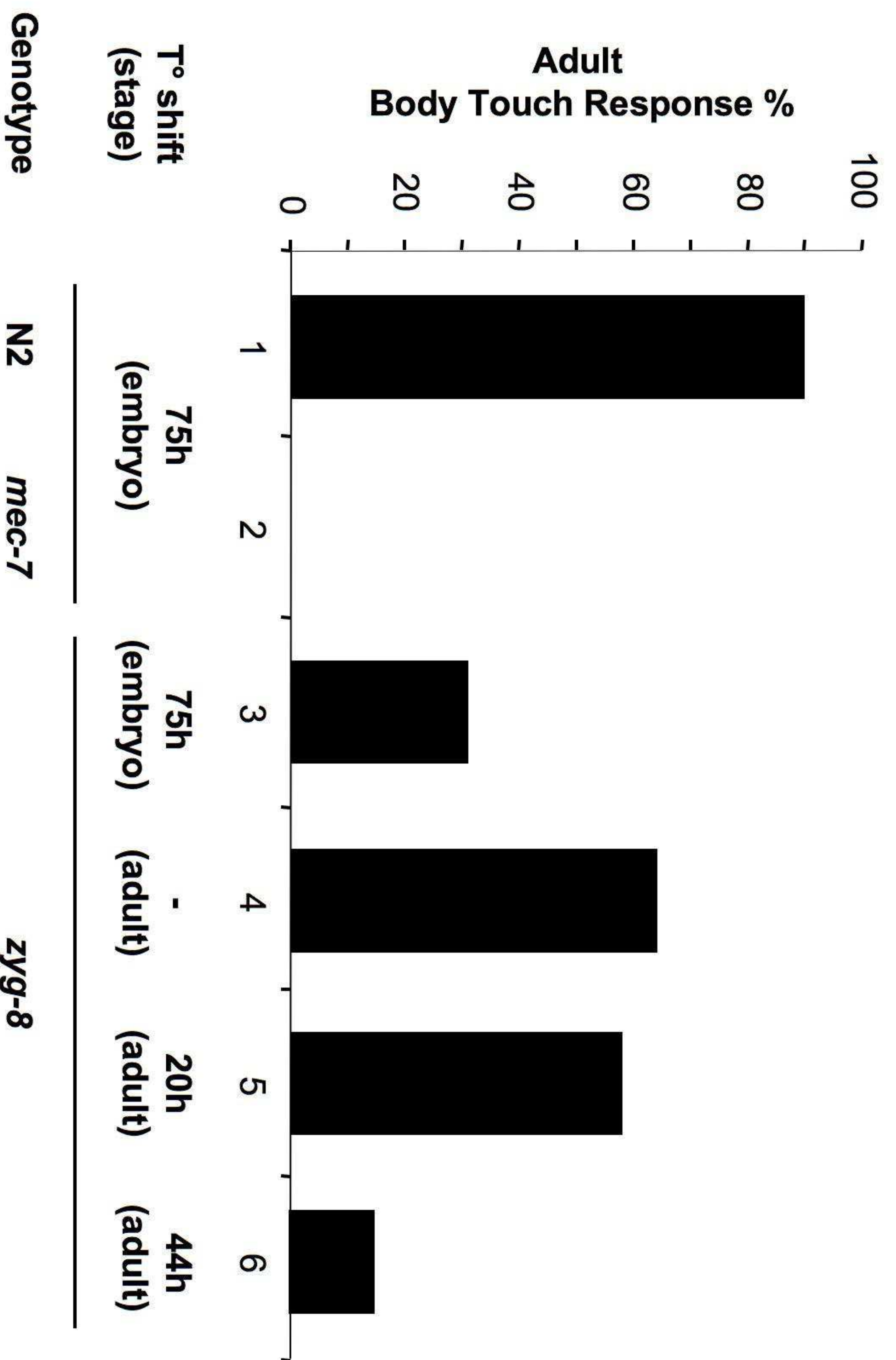
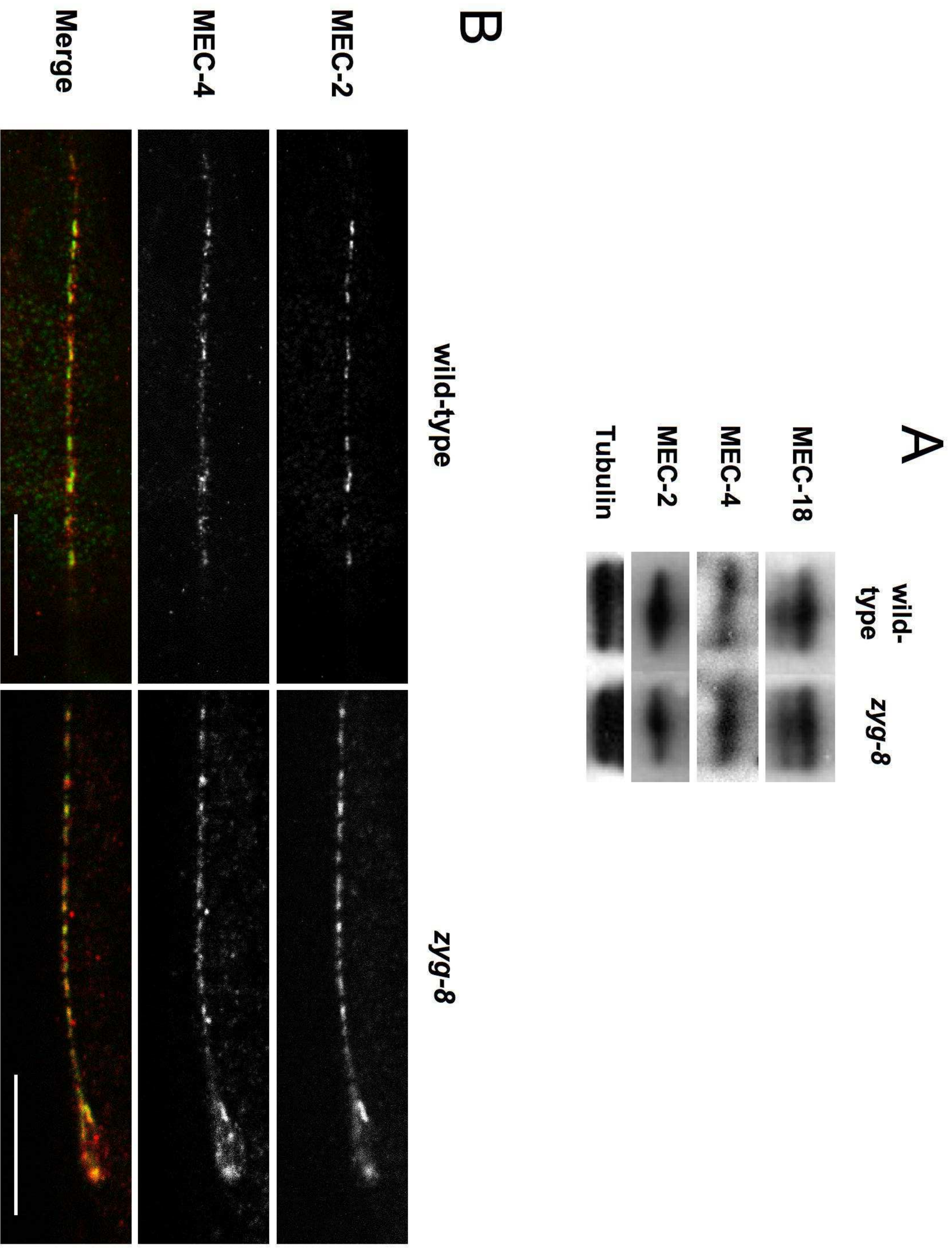


Figure 2





**Figure 4**

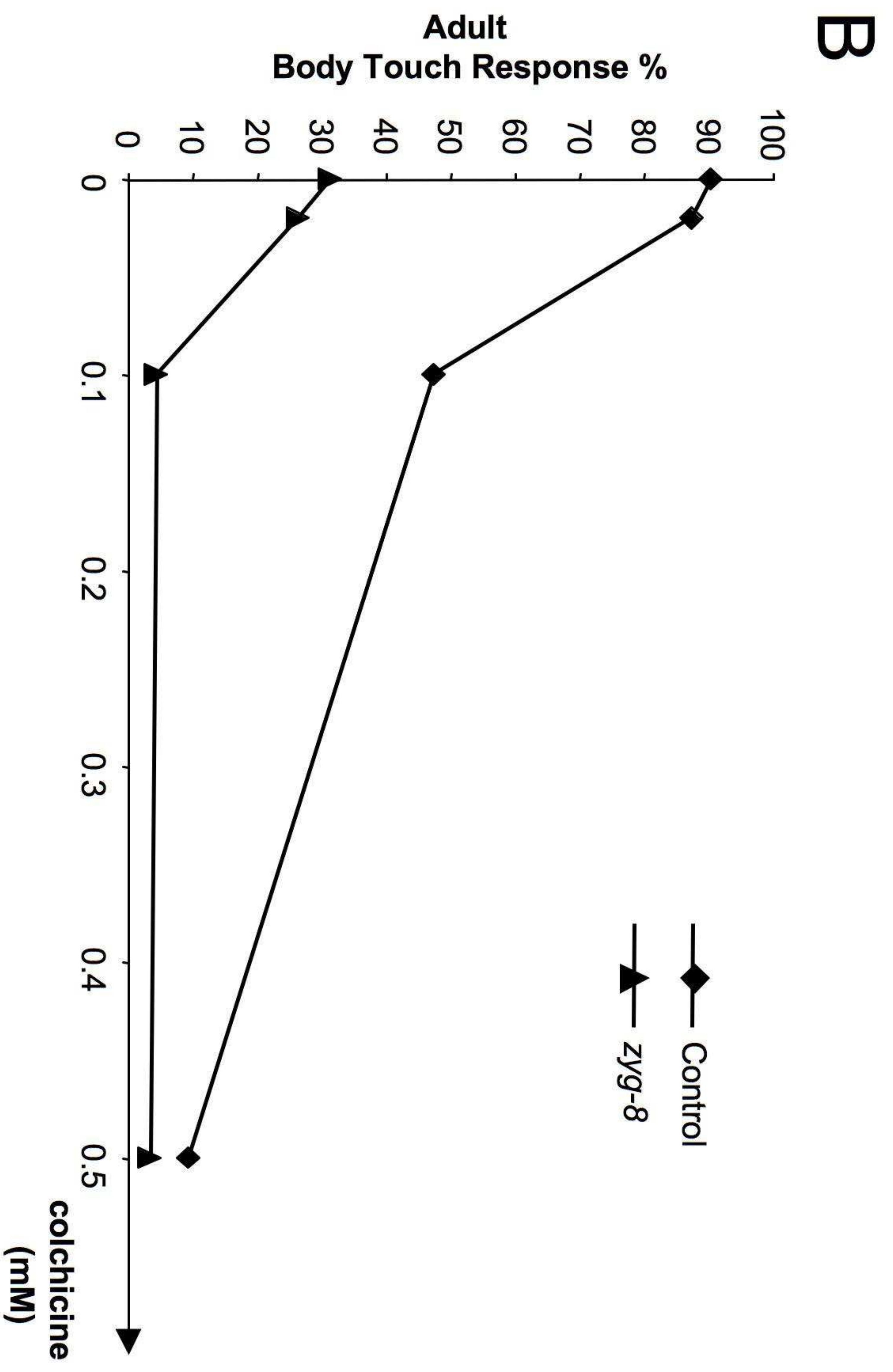
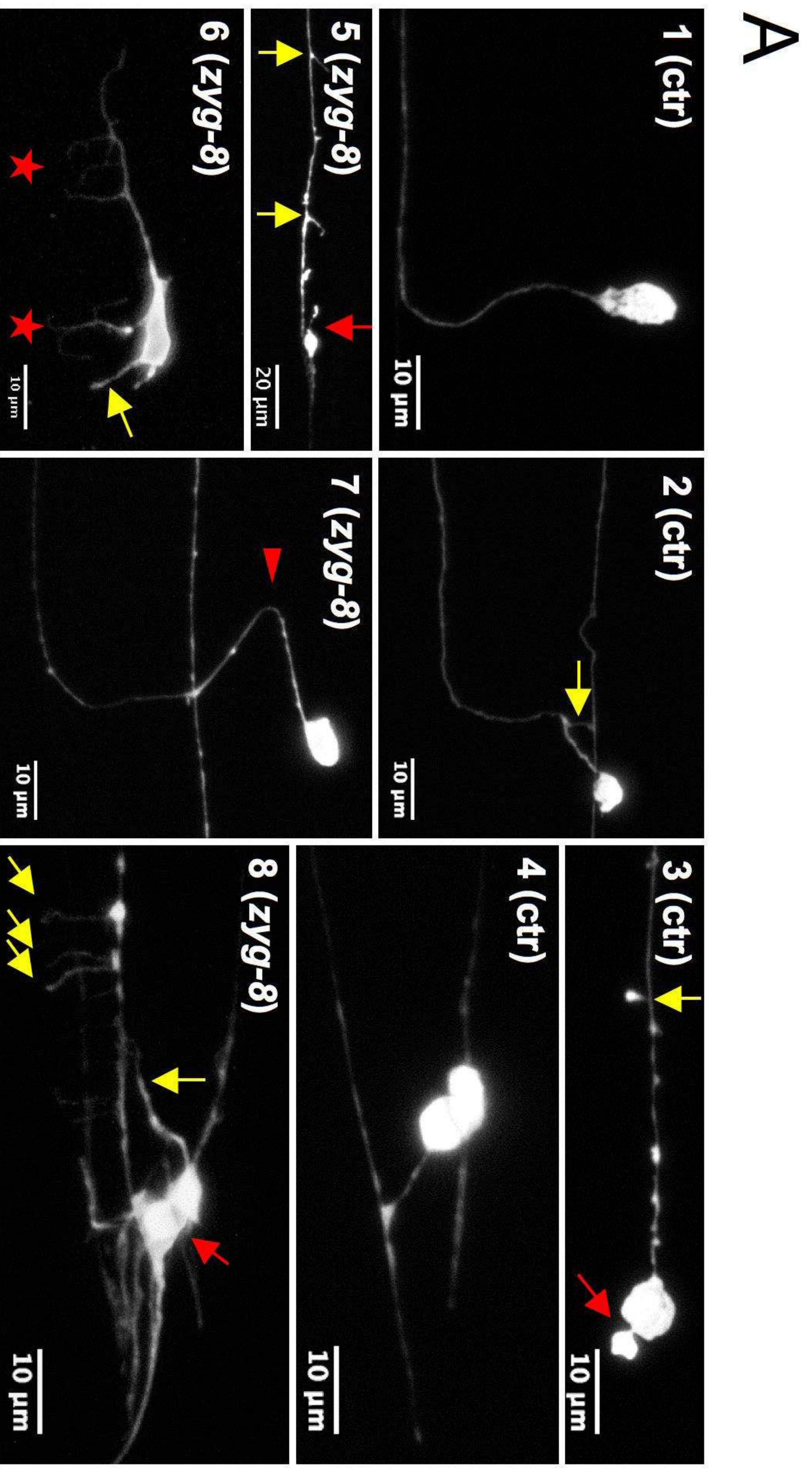
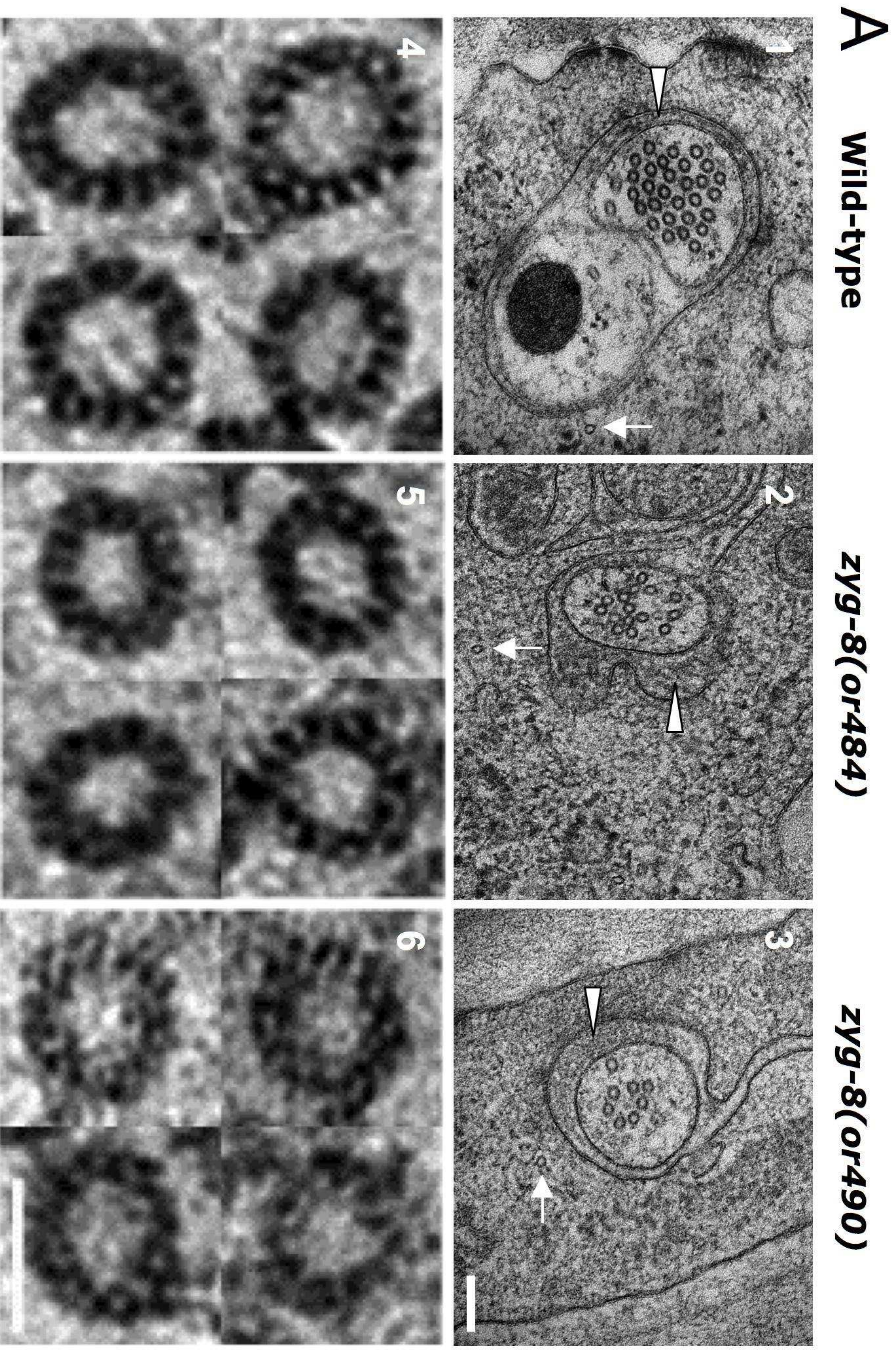
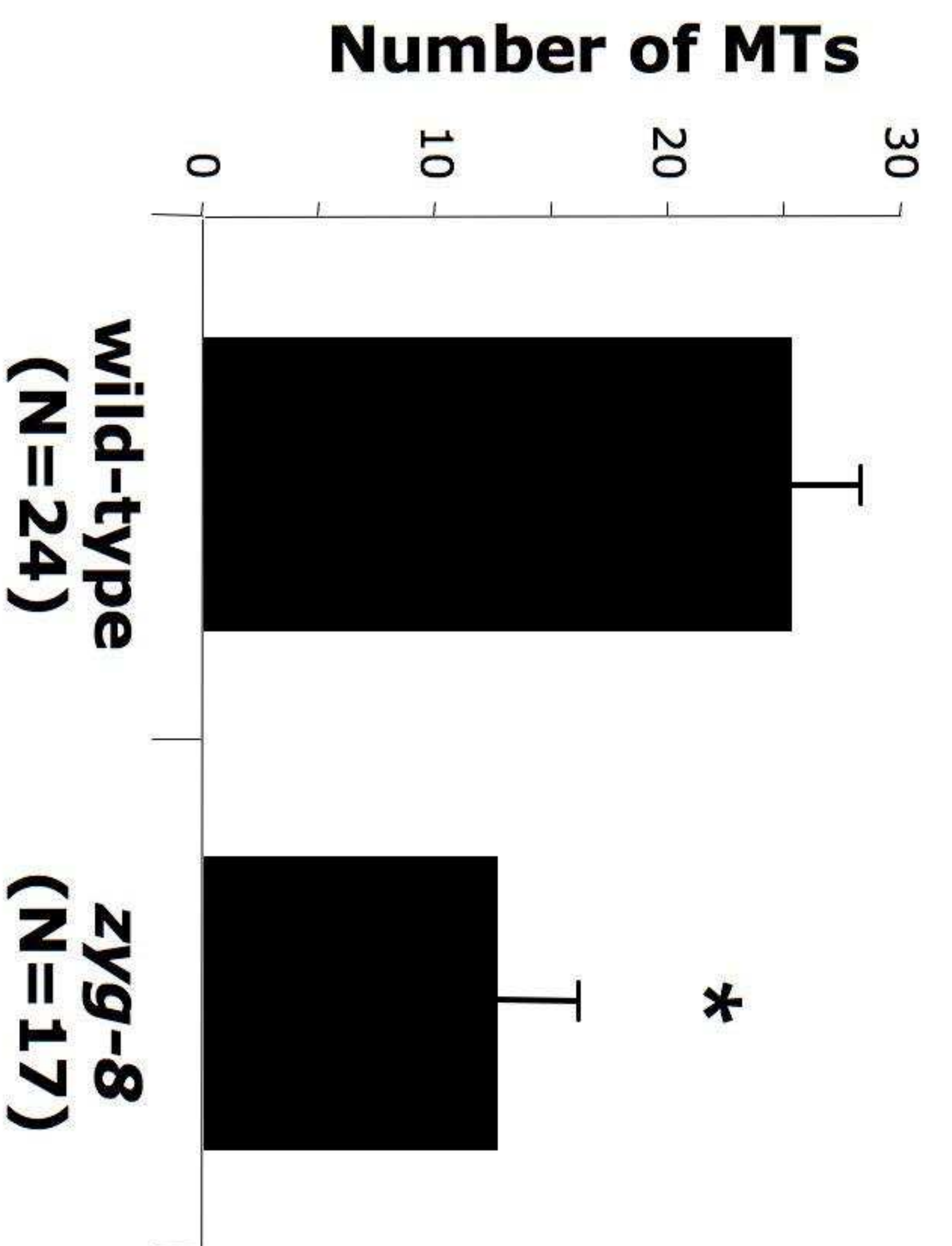


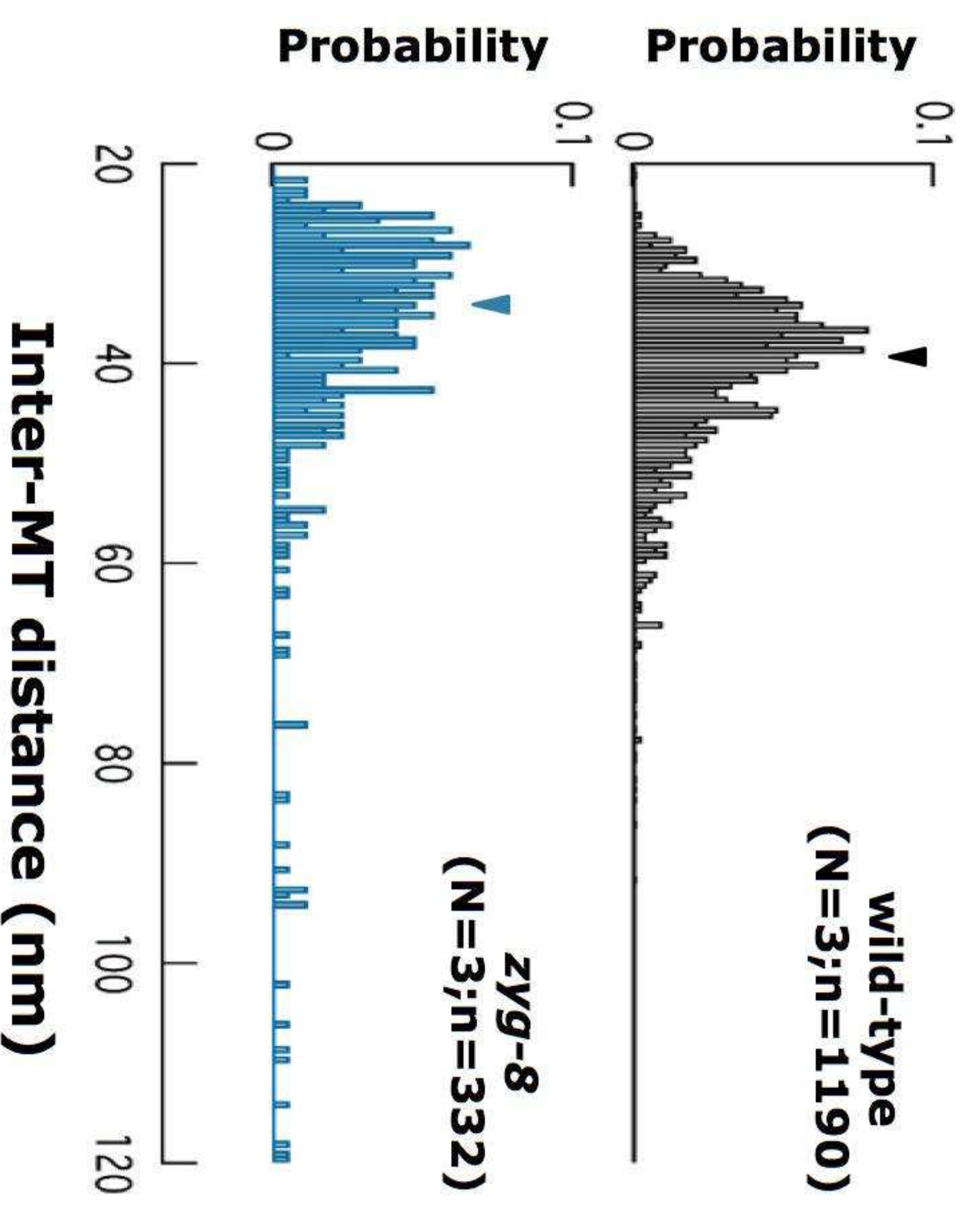
Figure 5



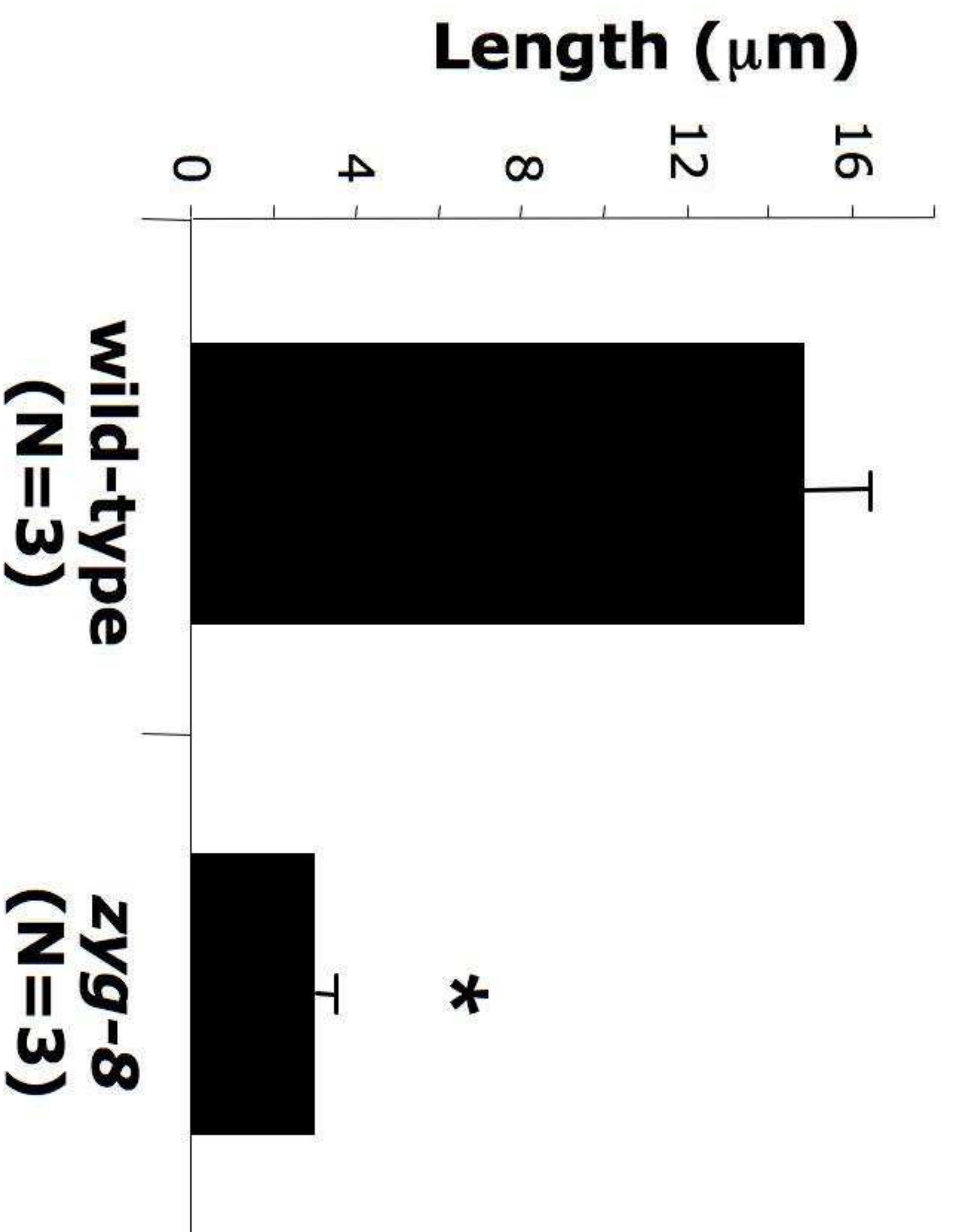
**B** TRN MT content



**C** TRN MT organization



**D** TRN MT length



**E** TRN MT caliber

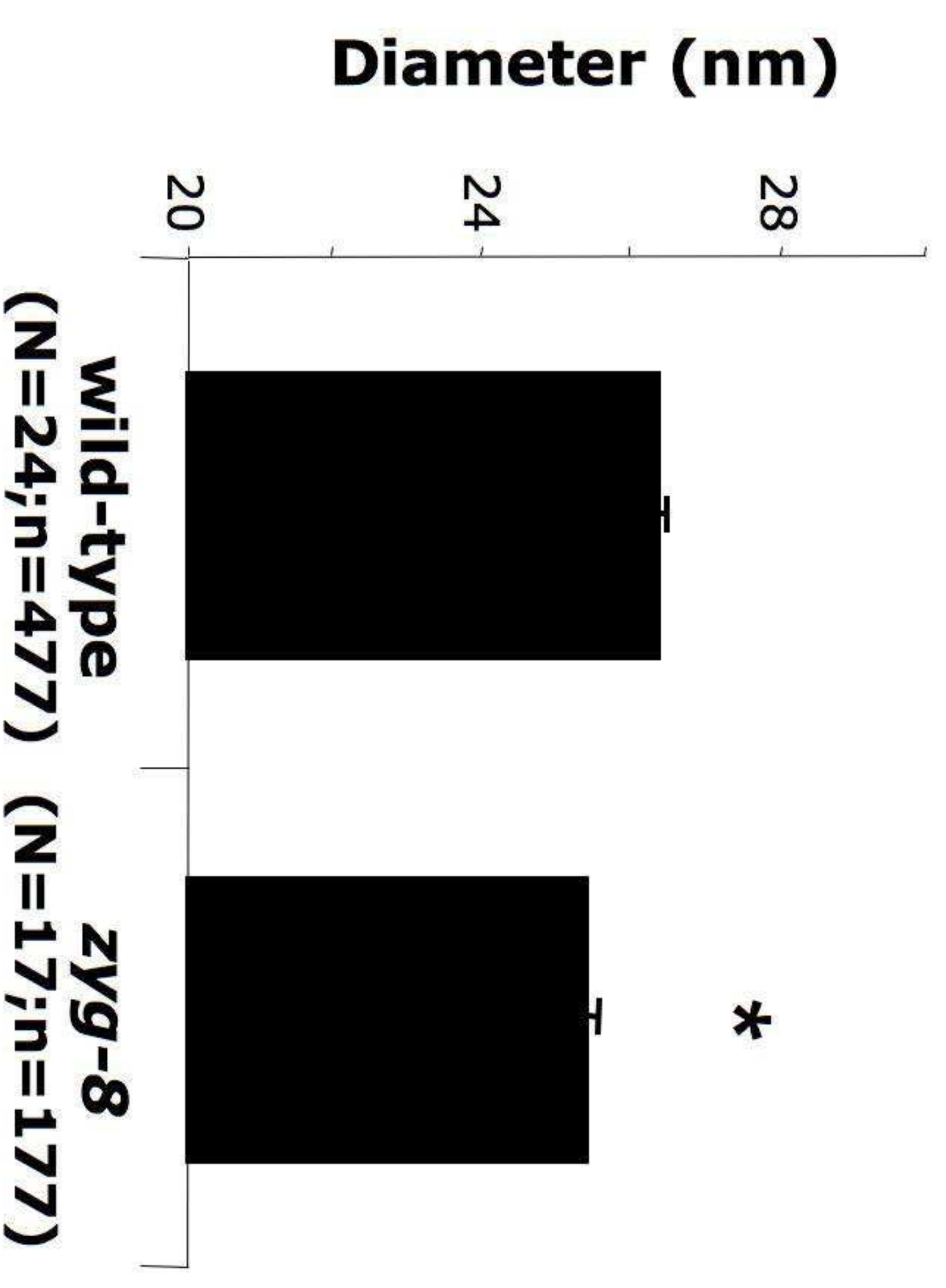


**Figure 6**

**Table 1. Touch Receptor Neuron Morphology & Outgrowth**

Genotype (25°C)	Morphology Defects (% animals, n = 25)						
	Cell Body			Process			
	Nb, position	Shape <sup>1</sup>	Polarity <sup>2</sup> (ALM)	Varicosities <sup>3</sup> (ALM;PLM)	Trajectory <sup>4</sup> (ALM;PVM ;PLM)	Ectopic branch	Lateral growth <sup>5</sup> (ALM;PLM)
<i>N2; zdis5</i>	0%	16%	24%	8%;0%	8%;0%;0%	16%	0%;0%
<i>zyg-8(or484); zdis5</i>	4%	40%	88%	20%;32%	8%;36%;20%	32%	56%;44%
<i>zyg-8(or490); zdis5</i>	8%	40%	92%	72%;100%	4%;36%;0%	12%	48%;60%

N2 (wildtype) and *zyg-8* alleles were crossed to *zdis5 [Pmec-4::GFP]* worms to visualize Touch Receptor Neuron morphology. Wildtype and mutant worms were cultivated at 15°C as described in Materials & Methods. Sets of N2, *or484* and *or490* late embryos were shifted to 25°C and 25 adult animals of each genotype were analyzed.

<sup>1</sup> Most of the cell bodies in control animals displayed a round and regular shape, as illustrated in Fig. 3A2-4. Defects scored here encompass irregular, elongated to spiky shapes.

<sup>2</sup> In our hands, control animals typically displayed bipolar ALM neurons due to a posterior extension longer than the cell body. *zyg-8* mutations reduced this posterior process. Occasionally, the polarity of other TRNs was altered in *zyg-8* mutants, as illustrated in Fig. 3A9 (PVM).

<sup>3</sup> Most of the TRN processes in control animals were straight and regular, as illustrated in Fig. 3A2-4. In contrast, *zyg-8* mutant animals displayed repeats of inflated areas along the processes of mostly PLM and AML, as illustrated in Fig. 3A5 and 3A7 (yellow arrowheads).

<sup>4</sup> Although TRN processes followed a straight ventral or anterior path in control animals, their trajectory in *zyg-8* mutants was altered, as exemplified by panel 6 of Fig. 3A. It is worth noting, however, that we could not find any case of missing connections.

<sup>5</sup> See Fig. 3A5, yellow arrow for an ALM cell.

**Table 2. Touch Receptor Neuron Synaptic Vesicles**

Genotype (L4s) <sup>1</sup>	°C	Synaptic Vesicle Defects (% animals, n = 35)			
		Nerve ring puncta			PLM puncta
		Nb	Diffuse/ localization	Size/spacing	Diffuse/ localization <sup>1</sup>
<i>N2; jsIs821</i>	15°	3%	14%	14%	6%
<i>N2; jsIs821</i>	25°	3%	17%	29%	6%
<i>zyg-8(or484); jsIs821</i>	15°	9%	32%	40%	9%
<i>zyg-8(or484); jsIs821</i>	25°	6%	37%	43%	29%
<i>zyg-8(or490); jsIs821</i>	15°	9%	26%	20%	9%
<i>zyg-8(or490); jsIs821</i>	25°	3%	43%	46%	23%

N2 (wildtype) and *zyg-8* alleles were crossed to [*Pmec-7::GFP-RAB-3*] worms to visualize Touch Receptor Neuron synaptic vesicles. Wildtype and mutant worms were cultivated at 15°C as described in Materials & Methods. Sets of N2, *or484* and *or490* late embryos were shifted to 25°C. Thirty-five worms of each genotype were analyzed as L4s, a larval stage at which the marker is more consistent and reliable.

<sup>1</sup> In wild-type L4 animals, GFP-RAB-3 appears as two strong puncta in the VNC, posterior to the vulva. Animals were scored for presence of diffuse GFP or additional very small puncta mislocalized along the VNC or in the PLM dendrites.

**Table 3. D Neuron Morphology & Outgrowth**

Genotype	°C	Morphology Defects (% animals)		
		Cell Bodies	Commissures	Fasciculation
<i>N2; juIs76</i>	15°	0/30 (0%)	0/30 (0%)	0/30 (0%)
<i>N2; juIs76</i>	25°	0/50 (0%)	0/50 (0%)	1/50 (2%)
<i>zyg-8(or484); juIs76</i>	15°	0/22 (0%)	2/22 (9%)	4/22 (18%)
<i>zyg-8(or484); juIs76</i>	25°	2/25 (8%)	3/25 (12%)	6/25 (24%)
<i>zyg-8(or490); juIs76</i>	15°	0/28 (0%)	2/28 (7%)	2/28 (7%)
<i>zyg-8(or490); juIs76</i>	25°	6/31 (19%)	5/31 (16%)	23/31 (74%)

N2 (wildtype) and *zyg-8* alleles were crossed to *juIs76* [*Punc25::GFP; lin-15*] worms to visualize GABAergic DD and VD motor neuron morphology. Wildtype and mutant worms were cultivated at 15°C as described in Materials & Methods. Sets of N2, *or484* and *or490* late embryos were shifted to 25°C while corresponding controls remained at 15°C. Six DD neurons extend axons during embryogenesis, and 13 VD neurons are born in L1 larvae and extend processes along the ventral and dorsal cord after the animals are shifted to 25°C. Adult worms were scored for alterations in cell body size and shape, commissures that were misplaced or extended along the wrong side of the body, and defasciculation of axons along the ventral and dorsal nerve cords.